Nano Research

Open Access

Review Article

Surface-enhanced Raman scattering on nanomaterials for cancer and pathogens diagnosis

Jingjing Wu[1,2,§], Baohong Zhang[4,§], Lei Xu[5], Yanyu Zhao[1,2], Tao Chen[3] ✉, Jie Lin[5] ✉, and Anran Li[1,2] ✉

[1] *School of Engineering Medicine, Beihang University, Beijing 100191, China*
[2] *Key Laboratory of Big Data-Based Precision Medicine, Ministry of Industry and Information Technology of the People's Republic of China, Beihang University, Beijing 100191, China*
[3] *School of Optics and Photonics, Beijing Institute of Technology, Beijing 100089, China*
[4] *Shanxi Lu'an Taihang Lubricant Technology Co., Ltd., Changzhi 046204, China*
[5] *Cixi Institute of Biomedical Engineering, Ningbo Institute of Materials Technology and Engineering, Chinese Academy of Sciences, Ningbo 315201, China*
§ *Jingjing Wu and Baohong Zhang contributed equally to this work.*

Cite this article: *Nano Research*, **2025**, *18*, 94907096. https://doi.org/10.26599/NR.2025.94907096

ABSTRACT: Surface-enhanced Raman scattering (SERS) is a non-invasive spectroscopic technique that provides specific chemical fingerprint information for biomarkers in cancer and pathogen diagnosis. However, the SERS strategies are limited by the non-specific interactions between substrates and co-existing substances in biological matrices and the challenges of obtaining molecular fingerprint information from the complex vibrational spectrum. In recent years, the rapid development of novel substrates with high SERS activity has opened up new opportunities for their applications in cancer and pathogen diagnosis. The aim of this review is to present the recent progress and perspectives of novel SERS-based substrates for cancer and pathogen diagnostic applications. First, we will introduce recently developed SERS-active nanomaterials and discuss the influencing factors of the SERS signals. Second, the advantages of SERS in the diagnosis of cancer and pathogens will be given. Third, we will review the latest breakthroughs in cancer and pathogen detection research with SERS technology, as well as the new opportunities for SERS applications brought about by artificial intelligence (AI) technology. In addition, the novel microfluidic-SERS platforms for cancer and pathogens diagnosis will also be discussed. Finally, we will summarize the challenges and future perspectives of SERS technology in the field of early cancer diagnosis and rapid pathogen detection. It is highly expected that this review could benefit a comprehensive understanding of the research status of the SERS-active nanomaterials and arouse the research enthusiasm for them, leading to accelerated clinical translation of SERS technology in cancer and pathogen diagnosis.

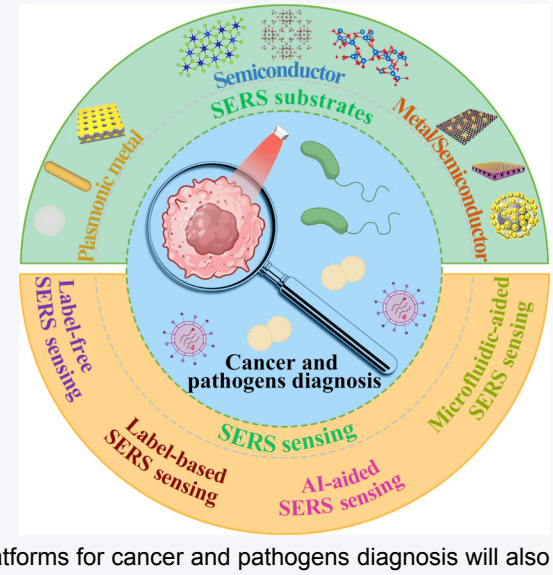

KEYWORDS: surface-enhanced Raman scattering (SERS), SERS-active nanomaterials, cancer and pathogen diagnosis, artificial intelligence (AI) technology

1 Introduction

Rapid diagnosis of diseases, including cancer and pathogens, presents a significant challenge for healthcare systems worldwide [1]. Early and accurate diagnosis of the disease is crucial for precision treatment and improved patient survival. However, very low concentrations of target biomarkers are frequently encountered in early cancer stages [2, 3]. Pathogens can be cultured *in vitro* to obtain sufficient cells, which improve the detection sensitivity. However, such complex procedures are prone to lengthy turnaround times for results [4–6]. Furthermore, diagnosing diseases is hindered by the inherent complexity of biological

Received: September 19, 2024; **Revised:** October 18, 2024
Accepted: October 26, 2024

✉Address correspondence to Tao Chen, 7420240004@bit.edu.cn; Jie Lin, linjie@nimte.ac.cn; Anran Li, rananli@buaa.edu.cn

samples [7–9]. Therefore, the detection of these target molecules requires more sensitive and precise techniques to ensure reliable diagnosis and monitoring.

Surface-enhanced Raman scattering (SERS) spectroscopy is a powerful vibrational spectroscopy technique that amplifies Raman scattering signals from target molecules by adsorbing them onto the surface of SERS-active nanomaterials. By designing the SERS substrate in a rational manner, the enhancement factor (EF) can reach up to 1×10^{10}–1×10^{14} [10]. This provides excellent sensitivity and an ultra-low limit of detection for the detection of target molecules at low concentrations. SERS has grown rapidly from theory to application since its discovery 50 years ago [11]. Due to its unique advantages, such as rapid and non-invasive detection, ultra-high sensitivity, and negligible photobleaching properties, SERS has gained popularity for the detection of biomarkers in cancer and pathogen diagnostics [12–16]. In fact, cancer and pathogenic cells, as well as their related biomarkers, are primarily composed of proteins or other organic molecules that possess intrinsic Raman signals, enabling direct detection and target identification based on the unique "fingerprint" information of their compositions. More importantly, the high sensitivity and fast detect feature provided by SERS are sufficient for diagnosing diseases even at a signal molecular level [17–19].

The sensitivity and reliability of SERS detection is highly dependent on the nature of the SERS substrate, including its composition, size, shape, structure, local environment, surface chemistry, and interaction with the target molecules. Therefore, designing, exploring, and constructing effective SERS substrates is the foundation and is with the utmost priority for the development and application of SERS technology. Generally, there are two types of SERS enhancement mechanisms: electromagnetic mechanism (EM) and chemical mechanism (CM). The EM contributes to SERS by strong Localized surface plasmon resonance (LSPR) is on the order of 1×10^{4}–1×10^{10}, while the CM induced by charge transfer (CT) resonance contributes to SERS approximately 10–1000 [20, 21]. In recent decades, SERS substrates have expanded from plasmonic metal nanomaterials to semiconductor nanomaterials and metal/semiconductor nanocomposites to achieve efficient SERS enhancement, improve detection sensitivity, and expand the range of their applications. Correspondingly, the SERS enhancement mechanism has also evolved from EM or CM alone to synergistic enhancement mechanism [22–25]. SERS technology holds great promise for the rapid and reliable diagnosis of cancer and pathogens through the efficient construction of SERS substrates.

The main advantage of SERS in the diagnosis of cancer and pathogens is that it allows direct and rapid detection of biomarkers by the specific Raman fingerprint of organisms [26–28]. Rich spectrum information provided by SERS enables further in-depth study of related disease at the molecular level [29, 30]. However, this label-free detection method faces challenges in the analysis and interpretation of spectral data when interfered by complicated biological matrices [31, 32]. One solution is performing indirect detection with SERS tags, which typically are composed of SERS active nanomaterials encapsulated with Raman reporter molecules that give strong and distinct Raman signals [33–35]. Further combined with specific recognition molecules, SERS tags can be highly selective for disease diagnosis even in complex matrices. Besides indirect detection strategies, the rapid development of the artificial intelligence (AI) technology has brought important opportunities for SERS. By employing machine learning algorithms (MLAs), large amounts of SERS spectral data can be used for automatic classification, pattern recognition, and feature extraction, leading to more accurate sample identification and detection. This approach provides a more efficient and intelligent method for the research and application of label-free SERS detection [36, 37].

This review gives a comprehensive discussion on the latest advances and prospects of SERS for cancer and pathogens detection (Fig. 1). We attempt to highlight diverse strategies to improve the SERS performance, hoping to provide readers with a reference for constructing a powerful SERS detection platform. Firstly, we will introduce the design and development of SERS-active nanomaterials, ranging from plasmonic metal nanomaterials, semiconductor nanomaterials, to the nanocomposites composed by them, and discuss the factors that influence their SERS activity. Secondly, we will present the advantages of SERS in diagnosing cancers and pathogens. Thirdly, we will review recent breakthroughs in cancer and pathogen detection research using SERS technology, as well as the new opportunities that AI technology offers for SERS applications. In addition, the novel microfluidic-SERS platforms with better reproducibility for cancer and pathogens diagnosis in real samples will be discussed. Finally, we will summarize the challenges and future prospects of SERS technology in the field of early cancer diagnosis and rapid pathogen detection.

2 SERS-active nanomaterials

Research on SERS technology has progressed rapidly since the SERS phenomenon was first observed in 1974 [38]. From then on, SERS substrates for Raman signal enhancement have been widely explored. Initially, precious metal nanomaterials like Au, Ag, and Cu were chosen as SERS substrates due to their unique physical properties, i.e., the negative real dielectric function and small positive imaginary dielectric function, that result in strong LSPR [16, 39]. With the continuous and rapid development of nanotechnology, SERS-active nanomaterials are no longer limited to plasmonic metal nanomaterials. Semiconductor nanomaterials and metal/semiconductor nanocomposites have also been proposed by researchers as efficient SERS substrates. This section will discuss the recent research progress on these three types of commonly used SERS substrates (Table 1).

2.1 Plasmonic metal nanomaterials

The SERS effect on plasmonic metal nanomaterials is primarily attributed to the EM, which refers to the enhancement of the local electromagnetic field induced by plasmonic resonance excitation [20, 40–43]. When the incident light interacts with plasmonic metal nanostructures, conducting electrons within the plasma metal nanomaterials can be driven to generate collective oscillations, resulting in local electromagnetic field enhancement. When Raman scattering occurs within this local enhanced electromagnetic field, it leads to a significant enhancement of the Raman signal of the molecules (Fig. 2(a)) [44]. A variety of plasmonic metal nanomaterials have been investigated as SERS substrates based on their ability to concentrate electromagnetic fields within a nanoscale range. Among them, Au, Ag, and Cu are commonly used SERS substrates for the enhancement of Raman signals from biological sources. Au has outstanding chemical stability and low biotoxicity [33]. Although not as stable as Au, Ag has a lower imaginary part of the dielectric function in the visible and near-infrared regions, which makes Ag more likely to acquire a stronger local electromagnetic field and higher SERS enhancement [45]. Cu is a

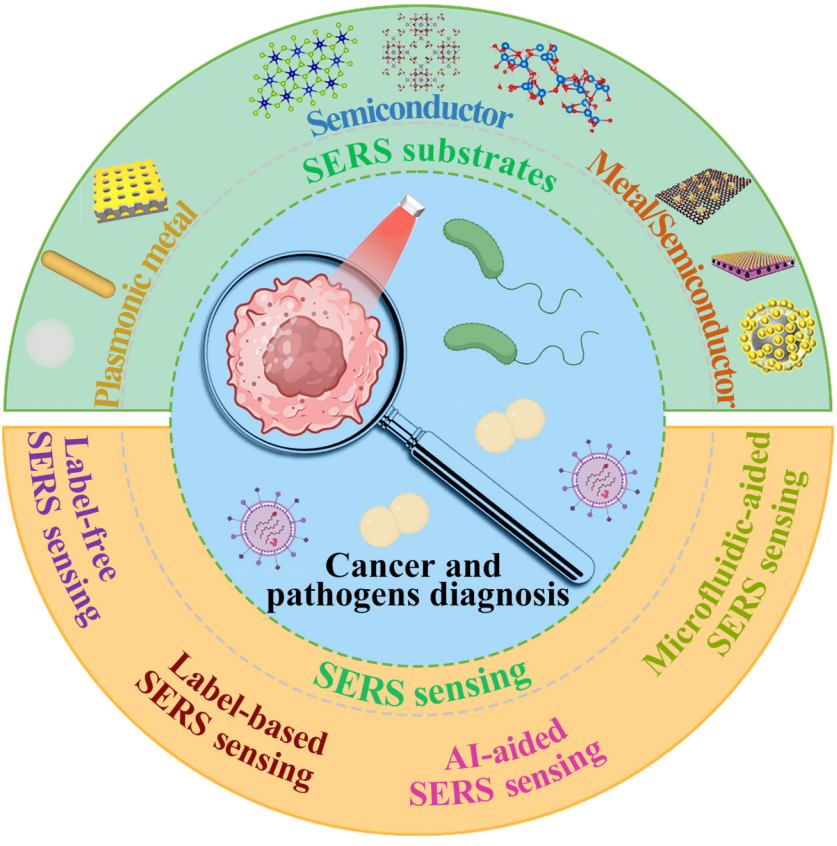

Figure 1 Schematic illustration of SERS strategies for cancer and pathogens diagnosis.

Table 1 Summary of several representative SERS-active nanomaterials and the corresponding SERS enhancement mechanisms as well as strategies to enhance the SERS activity

Type of nanostructure	Enhancement mechanisms	Strategies to improve SERS activity	Representative materials	Reporter	EF	Advantage	Potential weaknesses	Ref.
Plasmonic metal	EM	Size effect	150 nm Ag nanospheres	Py	~ 1×10^8	Excellent SERS sensitivity	Fabrication cost	[51]
		Shape effect	Ag nanocubes	CV	~ 3.1×10^5			[53]
		Constituent effect	Au/Ag nanostar	TFMBA	1.49×10^6			[63]
		Aggregation effect	AgFON	Rh6G	4.3×10^6			[81]
Semiconductor	CM	Defect engineering	α-MoO_{3-x} nanobelts	Rh6G	1.8×10^7	Selectivity; high stability; good biocompatibility; low cost-effectiveness	SERS sensitivity	[98]
		Elemental doping	Ga-doped ZnO	MPy	6.66×10^4			[105]
		Interface engineering	CuO/TiO_2 p-n heterojunction	4-MBA	8.87×10^6			[109]
		Phase transition engineering	$TaSe_2$ with a mixed structure of 2H to 1T (4:1) phase	Rh6G	1.5×10^5			[115]
Metal/ semiconductor	EM and CM	The optimization of each component in nanocomposites	2D Au/$PdSe_2$	Rh6G	4.5×10^5	Improved SERS activity; good reproducibility; high stability; selectivity	Controllable construction; mechanism elucidation	[123]
		Take advantage of the inherent properties of each component in nanocomposites	Magnetic Fe_3O_4-Au	Rh6G	1.4×10^8			[131]

superior alternative to Au and Ag for use in SERS-active nanomaterials due to its cost-effectiveness and abundance [46]. In addition to Au, Ag, and Cu nanostructures, other metals such as Al, Pt, Fe, Co, Ni, Ru, Rh, and Pd have also been synthesized for SERS substrates. Al nanostructures also have considerable EF values up to 1×10^4–1×10^6 compared to Ag, Au, and Cu nanostructures [47–49]. It is regrettable that Al is only suitable for applications in the ultraviolet (UV) region. Besides this, the availability of Al is also

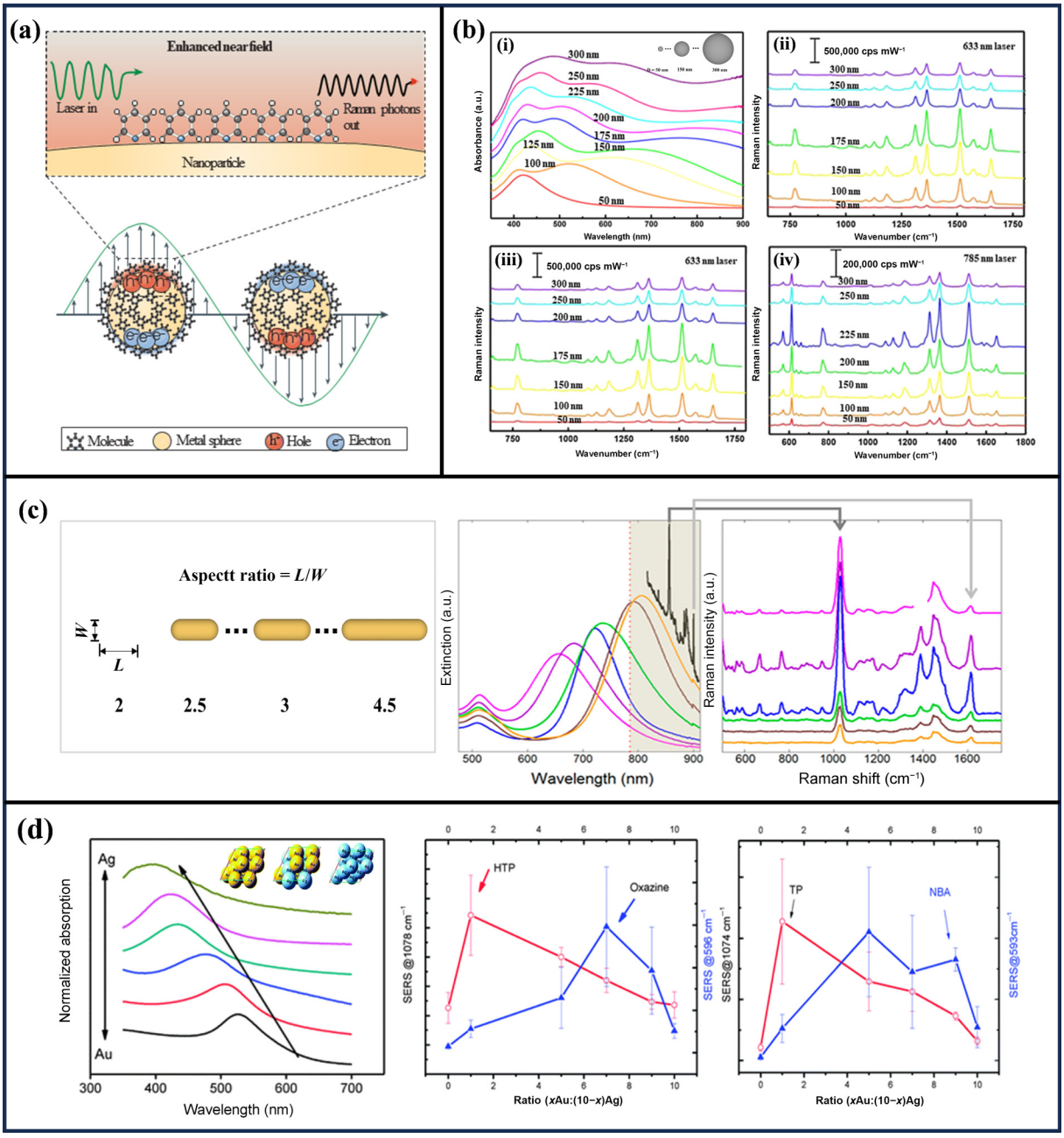

Figure 2 The SERS effect on plasmonic metal monomer. (a) Electromagnetic EM of plasmonic NPs. Reproduced with permission from Ref. [44], © Macmillan Publishers Limited 2016. (b) UV–Visible absorption spectra of Ag NPs with different sizes (inset: illustration of Ag nanospheres with increasing sizes). Raman spectra of Rh6G on Ag NPs with different sizes under different lasers: 532, 633, and 785 nm. Reproduced with permission from Ref. [51], © John Wiley & Sons, Lnd 2016. (c) Illustration of Au NRs with different aspect ratios. The extinction spectra of Au NRs with different aspect ratios (AR 2, pink; AR 2.5, purple; AR 2.75, blue; AR 3, green; AR 3.5, brown; and AR 4.5, orange) and the corresponding SERS spectra of methylene blue under different laser excitation. Reproduced with permission from Ref. [52], © American Chemical Society 2013. (d) UV–Visible extinction spectra of the Au_xAg_{10-x} NPs. From top to bottom: Ag, Au_1Ag_9, Au_5Ag_5, Au_7Ag_3, Au_9Ag_1, and Au (inset: models used in the DFT calculations of Au, Au-Ag, and Ag). Dependence of the SERS signal on the molar ratio of Ag to Au. Reproduced with permission from Ref. [55], © The Royal Society of Chemistry 2013.

limited due to surface oxidation and stability issues. While other transition metals such as Pt, Fe, Co, Ni, Ru, Rh, and Pd may not be as attractive as conventional SERS substrates due to their weaker SERS effect, nanostructures of these metals have shown the potential to provide sufficient enhancement for particular applications. Previous research has shown that SPR decides the huge enhancement of Raman signals in SERS. Therefore, precise control of the properties of the plasmonic metal SERS substrate, such as sizes, shapes, constituents, and arrangements, which directly affect the intensity and position of SPR, is essential for achieving efficient SERS activity [50].

2.1.1 *Size effect*

Au and Ag nanospheres are widely used as SERS substrates due to their fabrication flexibility. The plasma resonance effect of these isotropic nanospheres in a given dielectric environment depends

mainly on their sizes. Au and Ag nanospheres with a diameter of a few tens of nanometers in aqueous solution show an extinction band in the green and blue region, respectively, ascribing to their dipole plasmon resonance. As the particle size increases, the dipole plasmon resonance red-shifts and broadens, while higher-order multipole plasmon resonances are excited at shorter wavelengths. By optimizing the dimensions of Au and Ag nanospheres at a given laser wavelength, a higher electromagnetic enhancement can be achieved. For example, Tian et al. fabricated quasi-spherical Ag nanospheres with sizes ranging from 50 to 300 nm using a seed-mediated method [51]. The most remarkable SERS enhancement to Rh6G was observed from Ag nanospheres with a size of 150 nm when excited by a 532 nm laser. The maximum enhancement was observed from Ag nanospheres with a size of 175 and 225 nm when excited by a 633 and 785 nm laser, respectively (Fig. 2(b)). Note that the plasmon coupling effect of the surrounding precious metal NPs under SERS detection conditions can lead to a red-shift of the dipole, quadrupole, and higher-order modes in absorption band.

2.1.2 *Shape effect*

Compared to isotropic spherical NPs, anisotropic Au and Ag nanoparticles offer distinct advantages. Their higher curvature regions allow for greater tunability of plasmon resonance and higher EM enhancement. For example, by controlling the aspect ratio of Au and Ag nanorods (NRs), their plasmon resonance peaks can be finely tailored from the visible to the near-infrared range. Murphy et al. investigated the dependence of the plasmon resonance frequency of Au NRs on the aspect ratio [52]. They found that these NRs produced longitudinal surface plasmon resonances in the wavelength range of 600–800 nm and could generate intense electric fields at the tips of the NRs. They also discovered that the optimal SERS sensing could be achieved using Au NRs with a lower aspect ratio (Fig. 2(c)). Similarly, other anisotropic Au and Ag NPs, such as nanocubes, nanostars, and nanoflowers, also exhibited shape-dependent plasmon resonances. The numerous sharp tips, edges, and gaps on their surfaces can generate a significant number of "hot spots" that dramatically enhance local electromagnetic fields. For example, Ma et al. prepared Ag nanocubes with abundant "hot spots" by the polyol method and found that the SERS enhancement effect of crystal violet (CV) was significantly higher on these Ag nanocubes than on Ag nanospheres [53]. Liz-Marzán et al. found that Au nanostars can provide superior SERS enhancement by adjusting the core size, tip length, and sharpness [54]. Furthermore, anisotropically structured NPs have higher surface-to-volume ratios than spherical NPs. This promotes higher attachment densities of Raman reporter molecules, amplifying the SERS signals along with the individual tips of the nanostructures.

2.1.3 *Constituent effect*

By regulating the constituents of the plasmonic metal nanoparticles, the electronic structure, dielectric function, and spatial arrangement pattern of plasmonic metal nanomaterials can be significantly altered, resulting in superior chemical and physical properties compared to single-component nanomaterials. For example, Brolo et al. demonstrated that the SERS performance of Au-Ag bimetallic alloy NPs is superior to that of pure Au or Ag [55]. The charge donation from Ag to Au atoms allows target molecule to bind selectively to different metal regions on the surface of the of the Au-Ag bimetallic alloy (Fig. 2(d)). The preferential bonding caused the positively charged probe molecules oxazine 720 (Oxa) and Nile Blue A (NBA) to show the strongest SERS signals on the Au-Ag bimetallic alloy NPs with higher Au content, whereas the 4-hydroxythiophenol (HTP) and thiophenol (TP) probe molecules showed the highest SERS signals on the Au-Ag bimetallic alloy NPs with the largest Ag content. Furthermore, by combining constituent modulation with precise manipulation of structure, distribution, and shape, it is possible to achieve broader tunable SPR properties and optimized SERS activity on plasmonic metal nanoparticles. As shown by Verbrggen et al., the spectral shifts of Au-Ag alloys and Au@Ag core-shell nanostructures were considerably different [56]. Specifically, the spectral red-shift of Au-Ag alloy NPs from pure Ag to Au was proportional to the amount of Au, whereas the spectral shift of Au@Ag core-shell NPs was not gradual and the LSPR wavelength of Au@Ag core-shell NPs was larger than that of alloy NPs with the same overall composition. Furthermore, Cui et al. discovered that the SERS activity of core-shell $Ag_{100-x}Au_x$ NPs for thiophenol and p-aminothiophenol was significantly influenced by the molar ratio of Ag to Au [29]. As the Au molar fraction increased, the SERS activity was enhanced first and then weakened. The maximum Raman signal intensity was observed at x = 18, which was 10 times higher than that of Ag colloid. This was due to the presence of some pinholes on the surface of the core-shell $Ag_{100-x}Au_x$ NPs, which acted as a hot spot for the enhancement of the electromagnetic fields. To further optimize the core-shell sensors, Liang et al. corrected the signal fluctuations between samples and measurement conditions by embedding an internal reference in the core-shell metal NPs. The prepared Au@DTNB@Ag core-shell NPs, where DTNB acts as a Raman standard, can effectively correct the SERS signals and thus improve the repeatability and accuracy of SERS sensors [57]. The poor SERS enhancement by other metals (e.g., Pt, Pd, and Ni) and the weak interactions between typical noble metal SERS substrates and analytes like oxygen result in a limited SERS sensitivity. To tackle these issues, Weaver et al. adopted a SERS-borrowing strategy in which the inactive metal shell can "borrow" the SERS activity of Au or Ag core, ultimately leading to improved SERS performance [58, 59]. Yang et al. further extended this strategy to transition metal surfaces by constructing core-shell NPs [60]. Recently, Zhu et al. fabricated Au@Pt core-shell NPs to directly detect and simultaneously identify multiple mitochondrial ROS in living cells using spectroscopy [61]. The Raman signals of multiple ROS adsorbed on the Pt surface were illuminated by the SERS enhancement borrowed from the Au core. Li et al. extended this strategy to the Au@PtNi nanostructure and effectively observed the catalytic process with SERS *in situ* [62]. Besides, combining constituent modulation with shape management has also been shown to further enhance SERS activity. For example, Wang et al. prepared Au-Ag NRs, nanoshells, nanoflowers, and nanostars by a one-pot strategy and found that by changing the shape of the plasmonic metal nanostructures, the peak position of the LSPR in the range of 551–693 nm could be modulated [63]. Further studies showed that Au-Ag nanostars exhibited the highest SERS activity and could be applied for DNA mutation detection.

2.1.4 *Aggregation effect*

To achieve more effective SERS enhancement, plasmonic metal nanoparticle aggregates, and assemblies are increasingly employed for SERS detection, as they can provide the necessary conjunctions and gaps as the "hot spots" regions [64–66]. For instance, Schatz et

al. conducted computational simulations to investigate the LSPR characteristics of both spherical and triangular Ag dimers [67]. The results indicate that Ag dimers exhibit a stronger local electromagnetic field enhancement compared to the sharp tips on the surface of NPs. Zheng et al. synthesized a mixed Au NPs (GMDT) of Au monomers (GM), Au dimers (GD), and Au trimers (GT) by adding sodium chloride in the liquid phase [68]. Compared with GM solution, it was found that a red-shift of the LSPR peak can be observed in the extinction spectrum of GMDT solution. Additionally, the GMDT showed a stronger SERS enhancement than the GM (Fig. 3(a)). The simulation results indicated that the largest enhancement of the local electromagnetic field is concentrated in the gap between GD and GT with an excitation wavelength of 632.8 nm. Van Duyne et al. engineered the aggregation of Au and Ag NPs by adding inorganic salts as aggregating agents in the liquid phase to form effective "hot spots" for SERS, resulting in extremely high SERS enhancement and even single-molecule level sensitivity [69]. Xie et al. prepared Pd nanocubes dimers with an ideal face-to-face configuration, connected by biphenyl-4,4'-dithiol (BPDT) with a gap distance of about 0.8 nm between the two cubes [70]. The highest EFs were found at the corners of this interstitial gap, with values of the EFs as high as 2.8×10^4. By combining DNA origami technology with spherical Au or Ag NPs, SERS-active DNA origami-based dimers were fabricated with nanometer precision gaps [71]. Subsequently, the SERS performance of dimers was investigated in detail, providing SERS signal EFs of up to 1×10^{11}.

Considering that the final aggregation state of NP aggregates is highly dependent on the experimental conditions, they generally show poor performance in terms of repeatability and reproducibility. In this case, self-assembly processes can regulate dispersed colloidal systems into well-organized structures or

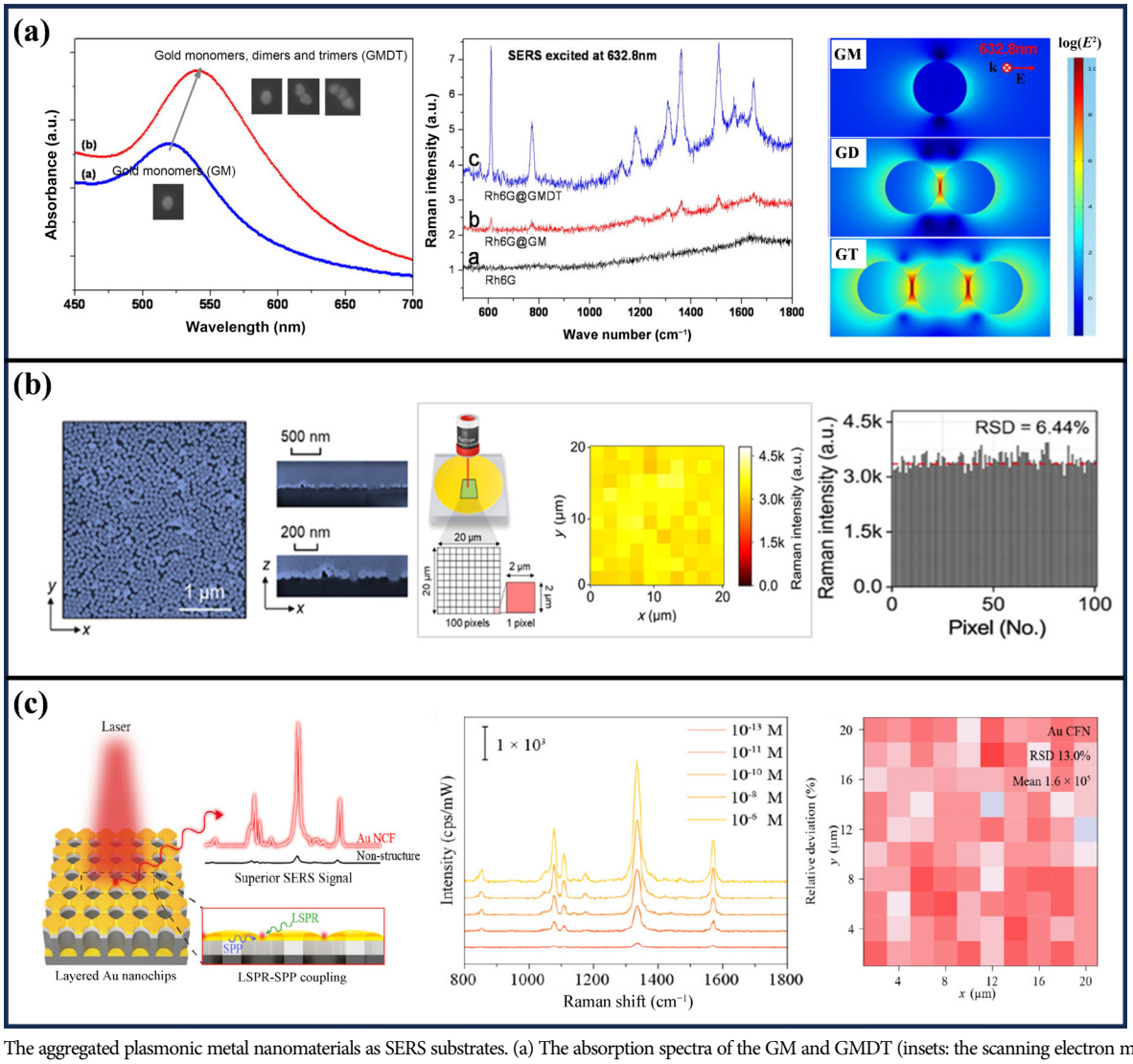

Figure 3 The aggregated plasmonic metal nanomaterials as SERS substrates. (a) The absorption spectra of the GM and GMDT (insets: the scanning electron microscopy (SEM) images of GM, GD, and GT); SERS spectra excited with 632.8 nm from Rh6G, GM, and GMDT; Images of the simulated distributions of $|E|^2$ were plotted in logarithmic scale with 632.8 nm excitation for GM, GD, GT and GMDT. Reproduced with permission from Ref. [68], © American Institute of Physics 2013. (b) Top and side views of SEM images for Au NPs with narrow nanogaps; Raman mapping images were measured by monitoring the Raman peak intensity variation at 1589 cm^{-1} of the Cy3 attached to the DNA terminal for 1 nM Cy3-DNA; RSD for the Raman peak intensities at 1589 cm^{-1} was determined as 6.44%. Reproduced with permission from Ref. [73], © American Chemical Society 2023. (c) Schematic illustration of Au CFN as SERS substrates; Raman spectra of 4-NTP at different concentrations absorbed on Au CFN; SERS mapping images of Au CFN at a wavenumber of 1340 cm^{-1} and the calculated RSD. Reproduced with permission from Ref. [76], © American Chemical Society 2023.

patterns without additional guidance. It is possible to precisely control the self-assembly of individual components in solution by modulating the functionality and affinity between NPs and solvent. For example, Galantini et al. exploited an approach in which specifically designed chiral co-surfactants are used to selectively deprotect the tips of Au NRs, thereby promoting selective tip-to-tip self-assembly of Au NRs [72]. It was further found that the assembled Au NRs exhibited a significantly higher number of optical hotspots than those assembled by the introduction of a conventional head-tail surfactant (sodium dodecyl sulphate (SDS) and bile salts (BS)). Choo et al. prepared an assembled layer of Au NPs with narrow nanogaps at the water-butanol interface by simple butanol dehydration (Fig. 3(b)). This innovative approach resulted in a highly sensitive, homogeneous and reproducible plasma SERS substrate with a relative standard deviation (RSD) of 6.44%. Further studies revealed that this SERS substrate can be used for the rapid detection of severe acute respiratory syndrome coronavirus 2 (SARS-CoV-2), with an extremely low limit of detection (LOD) of 3.1×10^{-15} M [73]. Self-assembly process via capillary forces is also one of the common strategies for fabricating close-packed plasmonic metal nanoparticle arrays. Lu et al. were the first to assemble Au trisoctahedra (TOH) with multiple tips in the capillary cube by electrostatic adsorption [74]. By systematically optimizing the size, density, and immersion time of the Au TOH on the glass surface, high activity (EF ~ 10^6) and good uniformity (RSD < 5%) of the prepared capillary-assisted substrate was obtained. Wang et al. embedded 4-MBA molecule as an internal reference in Au@Ag core-shell NRs [75]. The nanocomposites were further self-assembled by capillary force, and the obtained SERS substrate possessed richer SERS "hot spots", which reduced the RSD (RSD < 9.74%) and improved the detection sensitivity. However, the capillary force-driven self-assembly strategy suffers from a major disadvantage in that it is highly size-dependent and unable to be adapted to larger-sized NPs.

In addition to the self-assembly strategy, several techniques, including lithography and template, have also been developed to prepare a large number of uniform SERS substrates with excellent detection sensitivity, high stability and good reproducibility. Photolithography methods, including electron-beam lithography (EBL), optical lithography, and colloidal lithography, allows for a wide choice of geometries, delicate features, excellent signal reproducibility, and large-scale uniformity, giving this approach a special position in the development of SERS active substrates. Xiong et al. fabricated layered Au CFN (cap and film nanostructure) by means of a controllable electron beam lithography [76]. Benefiting from the remarkable electromagnetic field enhancement caused by the efficient LSPR-surface plasmon polariton (SPP) coupling at the structural junction of the Au cap and the Au film nanostructure, this SERS substrate obtains an EFs of 2.8×10^6 and a low LOD of 10^{-13} M employing 4-nitrothiophenol (4-NTP) as the probe molecule (Fig. 3(c)). Recently, Lu et al. used photolithography to produce patterned templates in which the assembly of Ag nanocubes was confined to each individual point of the pattern [77]. As a result, SERS substrates with high sensitivity (2.06×10^{-7} M) and high repeatability (RSD ~ 6.91%) were achieved. However, this strategy also has inherent disadvantages as it is time-consuming and expensive to implement. The templating approach typically uses closely packed polystyrene or silica nanospheres as templates [78–80]. Au or Ag is then formed by evaporation or sputtering onto the surface of the templates to form metal-film-over-nanosphere (MFON) substrates. The high SERS performance can be significantly improved by optimizing the size of the template sphere. According to Chiang et al., the optimal SERS signal with an EF of 4.3×10^6 was achieved using the AgFON substrate, drop-coated with polystyrene nanospheres of approximately 1000 nm in diameter, for a range of nanosphere sizes from 430 to 1500 nm diameters [81]. This was observed when the wavelength of the incident light was 532 nm.

2.2 Semiconductor nanomaterials

The study of the semiconductor nanomaterials with SERS activity dates back to the 1980s [38, 82]. Initially, researchers believed that semiconductor nanomaterials with SERS activity were limited to metal oxides, silver halides, and single-element inorganic nanomaterials such as Si and Ge [83]. After almost ten years of development, SERS has been successfully demonstrated on various semiconductor nanomaterials [84–87]. In addition to inorganic semiconductors, organic semiconductors have also been reported to serve as SERS substrates. For example, the nanostructured 1,10-(benzo[*b*]benzo[4,5]thieno[2,3-*d*]thiophene-2,7-diyl)bis(octan-1-one) (D(C7CO)-BTBT) film exhibited excellent SERS performance due to their lower LUMO orbitals, dipolar C=O···C=O interactions with target molecules, hydrogen bonds, and strong π-interactions that achieve an effective CT resonance [85]. Additionally, the EF values of these semiconductor nanomaterials have been increased from less than 1×10^3 to levels equivalent to those of Au and Ag nanostructures [88–90]. Furthermore, semiconductor nanomaterials with SERS activity offer several advantages over plasmonic metal SERS substrates, including low cost, simple preparation, large specific surface area, outstanding optical properties, and good biocompatibility. Their potential applications in SERS sensors are revolutionary.

The SERS effect on semiconductor nanomaterials is primarily attributed to the CM (Fig. 4(a)) [91]. Although this mechanism is not yet fully understood, there are three possible scenarios: (1) CT from the substrate to the target molecule by the incident beam with excitation resonance; (2) molecular resonance, where the target molecule is excited by the incident beam; and (3) enhancement due to non-resonant interactions between the surface and the adsorbed molecules. Therefore, achieving high SERS performance relies on the chemical interactions and energy level matching between semiconductor nanomaterials and target molecules [92–94]. Several strategies have been adopted to optimize the SERS performance of semiconductor substrates, such as defect engineering, elemental doping, interface engineering, phase transition engineering, size control, crystallinity regulation, and morphology control [23, 59, 83, 95–97].

2.2.1 *Defect engineering*

By introducing new energy states, defect engineering is performed to improve the SERS performance of semiconductor substrates [98, 99]. Oxygen vacancy and oxygen incorporation are the two primary methods of defect engineering. Zhao et al. discovered that Raman signals can be significantly enhanced by appropriately doping or extracting oxygen from semiconductor substrates [100]. Simulation and experimental results also show that adjustment of the energy level of the substrate by the incorporation or extraction of oxygen atoms in the semiconductor substrate lattice can modulate the positions of charge transfer transitions and exciton transitions to achieve SERS enhancement for specific molecules. Meanwhile, Li et al. proposed an effective electric current model based on the effective electric current in the photo-induced charge transfer

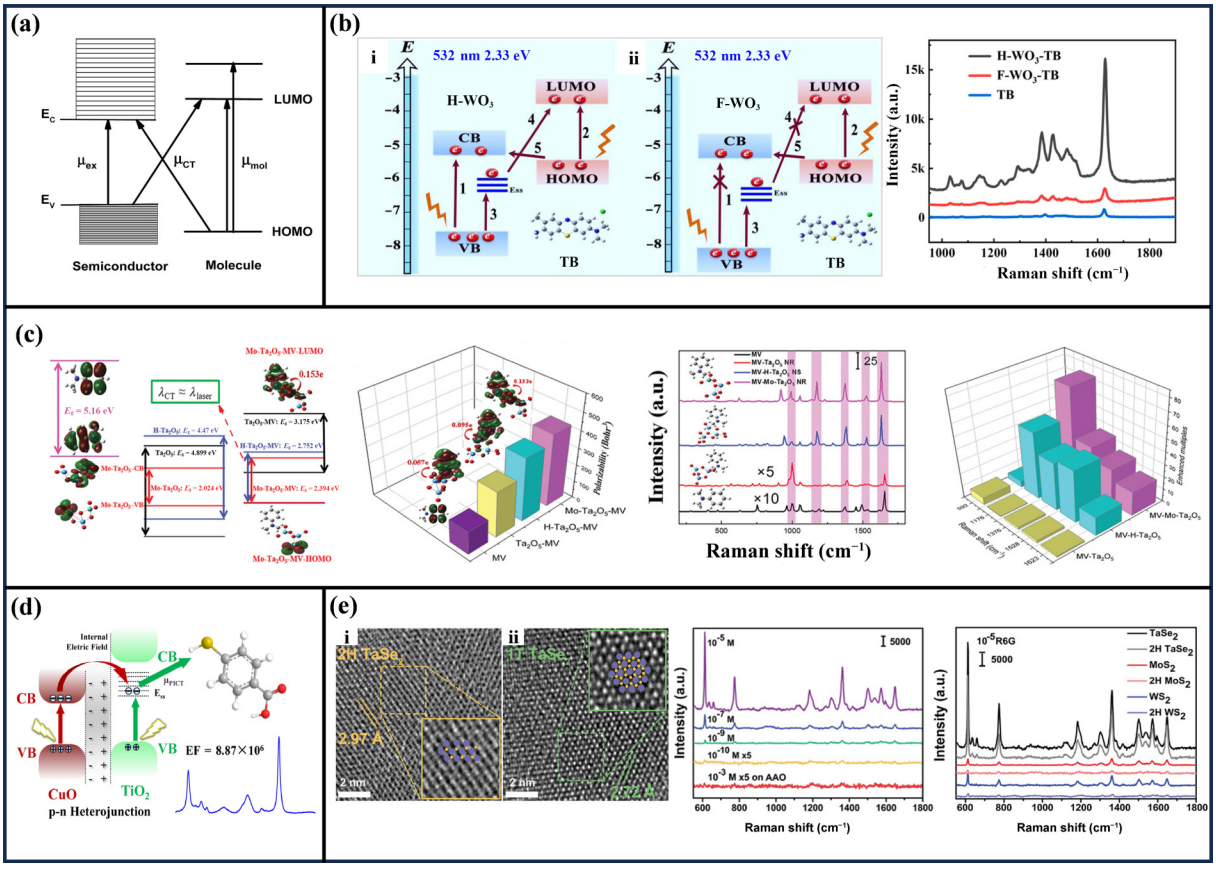

Figure 4 The SERS effect on non-metal nanomaterials. (a) Chemical enhancement mechanism (CM), reproduced with permission from Ref. [91], © American Chemical Society 2014. (b) Photo-induced CT process between H-WO_3 and TB and photo-induced CT process between F-WO_3 and TB; Raman spectra of TB (1.0×10^{-5} M) on H-WO_3, F-WO_3, and Si wafer. Reproduced with permission from Ref. [101], © American Chemical Society 2022. (c) The molecular orbital illustrations of the MV, different Ta_2O_5 clusters and MV-Ta_2O_5 complexes; calculated polarizabilities of the single MV, the MV adsorbed on Ta_2O_5 NR, H-Ta_2O_5, and the Mo-Ta_2O_5, respectively. The calculated static Raman spectrum of MV and MV on different Ta_2O_5 SERS substrates. Enhanced multiples of calculated Raman modes of MV at 992, 1176, 1376, 1528, and 1632 cm^{-1} on different Ta_2O_5 substrates. Reproduced with permission from Ref. [104], © Yang, L. et al. 2019. Published by WILEY-VCH Verlag GmbH & Co. KGaA, Weinheim. (d) Schematic illustration of CuO/TiO_2 p-n heterojunction as SERS substrates. Reproduced with permission from Ref. [109], © Published by Elsevier B.V. on behalf of Chinese Chemical Society and Institute of Materia Medica, Chinese Academy of Medical Sciences 2023. (e) HRTEM morphology of the $TaSe_2$ nanosheets with the ordered 2H phase and 1T phase. SERS signals for the Rh6G at different concentrations from 10^{-5} to 10^{-10} M. Comparison of the SERS performance of $TaSe_2$ with the MoS_2 and WS_2 and the pure 2H phase of $TaSe_2$, MoS_2, and WS_2. Reproduced with permission from Ref. [115], © Wiley-VCH GmbH 2022.

(PICT) process [98]. This model can quantitatively describe the PICT process between the substrate and the target molecule, as well as the oxygen vacancy concentration-dependent SERS enhancement in the semiconductor substrate. Therefore, it can predict the SERS behavior of other semiconductors. By modulating the concentration of oxygen vacancies, the SERS activity of α-MoO_{3-x} nanobelts was significantly enhanced, with EFs reaching as high as 1.8×10^7 and a LOD of 1×10^{-8} M for Rh6G. These results are comparable to those obtained with noble metal substrates. Additionally, optimizing the chemical synthesis conditions to generate surface defects can also greatly improve the SERS performance of semiconductor substrate. For instance, Yang et al. developed a simple template-free approach to produce WO_3 hollow microspheres (H-WO_3) assembled by nanosheets (NSs) [101]. This self-aggregation process resulted in several surface defects on the SERS substrate, leading to a significant increase in the SERS activity of H-WO_3 (Fig. 4(b)).

2.2.2 *Elemental doping*

Elemental doping strategy is another attractive route to improve the SERS activity of semiconductor substrates by tuning the energy band or increasing the concentration of free electrons [102, 103]. In the last few years, there have been reports on the enhancement of the SERS performance of semiconductors by doping strategies. For instance, Lombardi et al. reported a Mo-doped Ta_2O_5 semiconductor SERS substrate that exhibited significant SERS sensitivity to methyl violet (MV) molecules with an EFs of 2.2×10^7 by modulating the Mo doping concentration (Fig. 4(c)) [104]. This remarkable SERS effect can be rationally attributed to the "coupled resonance" strategy: (i) MV molecular resonance mechanism; (ii) PICT resonance between target molecule and SERS substrate; and (iii) electromagnetic enhancement in the gap and sharp tip of anisotropic Ta_2O_5 NRs. Similarly, Zhao et al. discovered that a Ga-doped ZnO substrate exhibits excellent SERS sensitivity to the 4-mercaptopyridine (MPy) molecule when excited by laser at 785 nm [105]. By modulating the Ga doping concentration, the EFs of the 5% Ga-doped ZnO substrate was found to reach as high as 6.66×10^4. Besides metal doping, non-metal doping has also been reported. Yamashita et al. reported a simple way to prepare a series of heavily hydrogen-doped semiconductors [106]. Among them, hydrogen molybdenum bronzes (H_xMoO_3) and hydrogen tungsten bronzes (H_xWO_3) exhibit strong visible plasma resonances,

resulting in high SERS activity. However, $H_xV_2O_5$ semiconductors cannot support plasma resonance. Therefore, it is crucial to select an appropriate substrate material for the doping strategy.

2.2.3 Interface engineering

Unlike defect engineering, interface engineering achieves charge concentration modulation without disrupting the crystal structure [107, 108]. The strong coupling at the heterojunction interface can enhance the separation efficiency of photogenerated carriers and promote effective CT, which is beneficial for SERS signals. For instance, Zhao et al. constructed a CuO/TiO_2 p-n heterojunction that exhibited a high EFs (8.87×10^6) for 4-mercaptobenzoic acid (4-MBA) [109]. This was mainly attributed to the internal electric field provided by the CuO/TiO_2 heterojunction interface and the strong interfacial coupling, which enhanced the charge collection ability and separation efficiency of photogenerated carriers (Fig. 4(d)). Recently, this group designed TiO_2/ZnO heterojunction as SERS substrate based on interface engineering strategy [110]. This substrate permitted the detection of antibiotic in eggs with a LOD of only 13.1 μg/kg, which is much lower than the European Union standard. The van der Waals (vdW) heterostructures are a type of vertical 2D heterostructure that rely on interlayer interactions dominated by vdW forces. Such heterostructures provide a distinct platform for SERS by combining various 2D materials with more complicated electronic structures. Chen et al. found that a graphene/WSe_2 vdW heterostructure could significantly amplify the SERS signal of CuPc through the CM, and the stacking sequence controlled the EFs due to the electron transition probability rates being affected by the different interlayer couplings [111]. In addition to improving CM, vdW heterostructures have also been reported to enhance EM. Wu et al. reported that TMD nanodome/graphene heterostructures could achieve highly sensitive SERS enhancement with a LOD as low as 1×10^{-12} M [112]. The researchers attributed the phenomenon to a combination of enhanced CM enhancement of dipole-dipole interactions at the TMD nanodome/graphene heterogeneous interface, and EM enhancement via LSPR on the photo-doped TMD nanodome/graphene.

2.2.4 Phase transition engineering

Recent studies have shown that phase transition engineering can greatly increase the Raman enhancement effect on semiconductor nanomaterials by manipulating their electronic structure. For example, Jin et al. discovered that the SERS activity of MoX_2 (X = S, Se) NSs can be significantly enhanced by the phase transition from the 2-hexagonal (2H)-to the 1-trigonal (1T)-phase [113]. First-principles density-functional theory (DFT) simulations suggested that the considerable enhancement of the Raman signals on metallic 1T-MoX_2 results from the facilitated CT from the Fermi energy level (E_f) of metallic 1T-MoX_2 to the highest occupied molecular orbital level (HOMO) of the adsorbed probe molecules, which is more efficiently performed than the process from the top of the valence band of semiconductor 2H-MoX_2. This work not only elucidates the mechanism of the Raman enhancement and identifies 1T-$MoSe_2$ and 1T-MoS_2 as potential SERS substrates, but also offers insight into the design of novel SERS substrates through phase transition engineering. Similarly, Xi et al. reported that the phases of transition metal nitrides also make a significant impact on the SERS performance [114]. The metallic δ-MoN as a SERS substrate achieved an LOD of 1×10^{-10} M and a strong EF of 8.16×10^6 for Rh6G. The outstanding SERS performance of δ-MoN can be attributed to the strong LSPR effect and the numerous of gaps and pores between the NSs, which easily generate electromagnetic "hot spots". Notably, the LSPR effect was crucial in achieving the superior SERS enhancement of δ-MoN. This is reported to be the first discovery of SPR-enhanced Raman enhancement in non-metal nanomaterials. With the development of different phases of semiconductor nanomaterials, a series of semiconductor with mixed-phase nanostructures have also been explored as SERS substrates. The semi-metallic $TaSe_2$ NSs with a mixed structure of 2H to 1T (4:1) phase was demonstrated as an excellent SERS substrate, and a LOD down to 10^{-9} M was obtained for Rh6G [115]. Surprisingly, the Raman enhancement of this SERS substrate is also the highest by comparing with pure 2H-$TaSe_2$, MoS_2 and WS_2 containing 1T and 2H phases, 2H-MoS_2 and 2H-WS_2 (Fig. 4(e)). The experiments and DFT simulations confirmed that the outstanding SERS properties of $TaSe_2$ NSs can be attributed to the strong adsorption energy and abundant electronic states near the E_f, which significantly increase the CT probability in the CM mechanism. Furthermore, the $TaSe_2$ NSs allowed for highly sensitive detection of bilirubin in serum and urine samples. It exhibited an excellent linear relationship and a low LOD of 0.316×10^{-6} M. This work is considered to offer an attractive avenue for applications in plasmon-free SERS detection of target of relevance in clinical diagnostics.

2.2.5 Other strategies

In addition to the above methods, other strategies have also been employed to improve the SERS performance of semiconductor substrates. such as: (1) Size control. Nanoparticle size is a crucial factor in determining SERS activity; in particular, when it is smaller than the exciton Bohr radius, the quantum confinement effect can result in a strongly size-dependent Raman spectra and higher SERS enhancement by fine-tuning the position of the band edge in semiconductors. For instance, Zhao et al. prepared three types of quantum dots with particle sizes ranging from 2 to 100 nm [116]. They discovered that $MoO_3 \cdot xH_2O$ quantum dots with a size of 2 nm generated vibronically coupled multi-pathways and highly efficient CT resonances due to the combination of the quantum size effect and the increasing concentration of lattice defects during the preparation process. This vibronic coupling between multi-resonant CT processes significantly improved the SERS performance of the $MoO_3 \cdot xH_2O$ quantum dots. (2) Crystallinity regulation. Guo et al. prepared amorphous ZnO nanocages (a-ZnO NCs) as SERS substrates, finding that amorphous materials facilitate surface electron escape and transfer due to their long-range disordered structure [117]. Systematic experiments and DFT calculations confirmed the significant SERS activity of the prepared amorphous a-ZnO NCs. The EF was as high as 6.62×10^5, which is higher than that of crystalline ZnO nanocages (c-ZnO NCs). (3) Morphology control. Two-dimensional (2D) non-metal nanomaterials have received considerable attention due to their unique thickness-dependent physicochemical properties, especially since the discovery of SERS activity in monolayer graphene by Liu et al. [118]. For example, atomically thin $TaSe_2$ as SERS substrate was fabricated for detecting various Raman-active molecules [115]. The excellent SERS performance of $TaSe_2$ is attributed to its large adsorption energy and a high number of filled electrons near the E_f. Qiu et al. also reported that the 2D $Mo_{4/3}B_2$ MBene nanomaterial exhibited superior SERS sensitivity compared to bulk MoB, with a

low LOD (10^{-10} M) and a high EF value (3.88×10^6) [99]. (4) Molecular enrichment. Metal-organic frameworks (MOFs) as SERS substrates have attracted significant attentions due to their molecular enrichment ability, selectivity, gas-sensitizing capability, and good chemical enhancement properties. Li et al. reported MIL-100 (Fe) SERS substrate with a LOD as low as 2.5 ppm to toluene [119]. Similarly, Jiang et al. demonstrated that Cu^{2+}-doped ZIF-67 substrates exhibited a high EF of 6.07×10^6, excellent detection sensitivity to MeB with LOD of 10^{-8} M, and fine reproducibility with an RSD of 14.1%, as well as excellent signal stability with an RSD of 2.59% [120]. (4) Environmental change. The low temperature has been confirmed to favor the SERS activity of semiconductors. Taking porous ZnO NSs as an example, Wu et al. found that low-temperature conditions effectively improve the interfacial PICT efficiency, thereby enhancing the SERS performance of the substrate [121].

2.3 Metal/semiconductor nanocomposites

The previous chapters discussed the SERS properties of plasmonic metal nanomaterials and semiconductor nanomaterials, respectively. semiconductor nanomaterials present major advantages such as selective Raman signal enhancement of target molecules, high stability, good biocompatibility, and low cost-effectiveness, but SERS sensitivity is still lower than that of plasmonic metal nanomaterials, such as Ag and Au nanostructures [122]. The extended construction of SERS-active nanomaterials from single-component to two or multi-components can therefore achieve the collective properties and performance enhancement of nanocomposites SERS platforms through the synergetic or complementary performance of different functional components. Furthermore, it is possible to overcome the limitations of plasmonic metal SERS-active substrates in terms of reproducibility, stability and selectivity by integrating them with other functional components. The integration of plasmonic metal and semiconductor nanomaterials is expected to provide synergistic SERS enhancements and new properties, thus providing a reliable approach for designing high performance SERS substrates. However, it is still crucial to explore the synergistic effect between EM and CM and further improve the SERS sensitivity of these nanocomposites.

The CT in the heterojunction interface of plasmonic metal and semiconductor nanostructures is highly dependent on the physicochemical properties of these nanocomposites, the probe molecule, and the assembly method. Therefore, the overall SERS performance can be significantly improved by optimizing various parameters, such as the properties of each component and excitation energy in these nanocomposites. Zhao et al. prepared AuNPs/$ReSe_2$, AuNPs/MoS_2, and AuNPs/$PdSe_2$ SERS hybrid substrates using Au-mediated mechanical exfoliation followed by appropriate etching in KI/I_2 solution [123]. The resulting SERS substrates had an LOD that was approximately 3 to 4 orders of magnitude lower than that of the bare 2D materials. Among three SERS hybrid substrates, Au NPs/$PdSe_2$ exhibited the optimal SERS performance, while AuNPs/$ReSe_2$ exhibited the worst SERS performance. The simulation results also show that Au NPs/$PdSe_2$ has the strongest electric field, while AuNPs/$ReSe_2$ has the weakest. Chen et al. reported that by modulating the thickness of the Cu_2S shell, the SPR resonance frequency and carrier distribution of the Ag/Cu_2S/4-MBA nanocomposite system can be effectively altered, leading to excellent SERS performance at various excitation energies [124]. Similarly, Fu et al. reported that CT contributes significantly to SERS in Ag/TiO_2/Ni nanopillar arrays at different laser wavelengths, showing a high TiO_2-thickness dependence [125]. Plasma metal-induced CT in SERS hybrid substrates can also be enhanced by a CM to improve overall SERS performance. For instance, Liu et al. produced Ag/ZnAl-LDH NSs using a simple one-pot solvothermal growth strategy [126]. The LOD was as low as 1×10^{-10} M, and the EFs was 1.7×10^5 when 4-nitrobenzenethiol (4-NBT) was employed as probe molecule. In this SERS hybrid system, laser irradiation generates hot electron-hole pairs, and the hot electrons are subsequently injected into the surface-state energy level (ESS) of ZnAl-LDH and the LUMO of the probe molecule. The addition of injected electrons improves the efficiency of PICT in the substrate, demonstrating the synergistic effect of Ag and ZnAl-LDH (Fig. 5(a)).

Hybrid substrates composed of plasmonic metal and photosensitive semiconductor nanomaterials can further enhance SERS performance through photoinduced enhanced Raman scattering (PIERS). This PIERS effect involves irradiating the substrate with a second light beam before or during Raman testing to promote the CT process between the semiconductor and the metal, resulting in increased Raman signals and improved sensitivity. For instance, Parkin et al. reported that the SERS signal was enhanced several times on Ag-TiO_2 substrates after a period of UV pre-irradiation [127]. The researchers suggested that the mechanism involved in PIERS is the UV-mediated migration of electrons from the semiconductor to the metal nanoparticles. This results in a stronger local EM field for the metal NPs, allowing more electrons to be transferred to the analyte via the CT process. Similarly, Li et al. combined TiO_2@Ag NP substrate with Au nanoprobes to form a sandwich nanocomposite, achieving increased sensitivity beyond the normal SERS effect under UV irradiation (Fig. 5(b)). This PIERS sensor is a useful tool for sensitively analyzing various biomolecules including adenosine triphosphate (ATP), thrombin, and cocaine [128].

In addition to participating in the CT process, semiconductor nanomaterials in hybrid SERS substrates also provide additional functions due to their inherent properties, such as interacting and selecting with target molecules differently than metal NPs, controlling the assembly of metal NPs, and protecting the surface of the plasmonic metal nanostructures. Yamauchi et al. combined mesoporous plasmonic Au films with microporous homochiral metal-organic frameworks (HMOFs) to prepare hierarchical porous hybrid films [129]. The hybrid SERS substrates allow for extremely low LOD for pseudoephedrine in undiluted blood plasma. This is due to dual enhancement mechanisms, namely physical enhancement by the mesoporous Au nanostructures and chemical enhancement by HMOF. Additionally, the chemical recognition by microporous AlaZnCl HMOF and a discriminant function for bio-samples containing large biomolecules, such as blood components, contribute to the substrate performance. Yang et al. self-assembled Au nanospheres into Au nanosphere monolayer, which was subsequently coated with a thin silicon shell to which polydimethylsiloxane (PDMS) brush was grafted [130]. The silica shell acts as a bridge between the Au nanosphere monolayer and the PDMS brush layer, and also anchors the Au nanosphere to the silicon wafer. Single-layer PDMS brush smooths the Au nanosphere monolayer, making it easy to clean and reuse. Additionally, the smooth surface of the SERS substrate enables the concentration of analytes in solution into small areas during solvent evaporation,

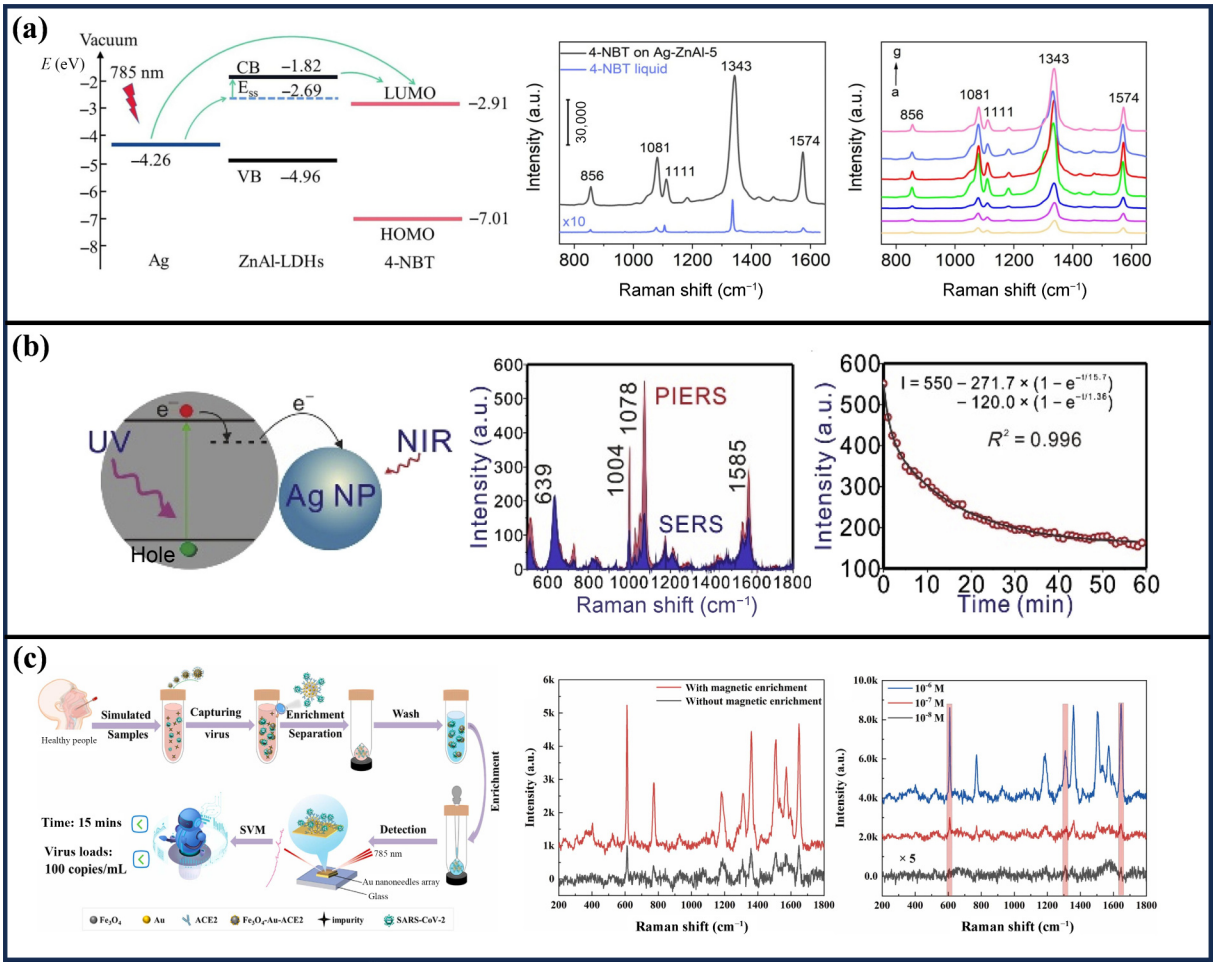

Figure 5 The SERS effect on metal/non-metal nanocomposites. (a) Schematic diagram illustrates the photo-induced CT process between 4-NBT molecules and Ag-ZnAl hybrid substrate under the excitation of 785 nm laser. Raman spectra of 4-NBT adsorbed on Ag-ZnAl-5 and 4-NBT solution dropped on Al foil, and different concentrations of 4-NBT adsorbed on Ag-ZnAl-5, where curves a to g corresponds to 10^{-5} to 10^{-10} M. Reproduced with permission from Ref. [126], © Elsevier B.V. 2022. (b) The schematic of PIERS via a CT. The comparison of PIERS spectra and SERS spectra for 4-MBA on TiO_2@AgNP substrate. A time-dependent PIERS signal at 1078 cm^{-1} of 4-MBA on TiO_2@AgNP substrate after ultraviolet irradiation. Reproduced with permission from Ref. [128], © Elsevier B.V. 2019. (c) The schematic diagram of magnetic SERS biosensor structure for SARS-CoV-2 virus detection. The SERS spectra of 10^{-6} M Rh6G by Fe_3O_4-Au nanocomposite with magnetic enrichment (red line) and without magnetic enrichment (black line). The SERS spectra of Rh6G solutions with concentrations ranging from 10^{-6} to 10^{-8} M. Reproduced with permission from Ref. [131], © Elsevier B.V. 2022.

significantly enhancing their SERS enhancement. Efficient collection and control of plasmonic NPs can also enhance SERS activity. By combining plasmonic NPs with magnetic nanomaterials, it is possible to control and collect SERS substrates using an external magnetic field. For example, Yang et al. reported angiotensin-converting enzyme 2 (ACE2)-modified Fe_3O_4-Au nanocomposites in which the magnetic property of Fe_3O_4, the SERS activity of Au NPs, and the viral trapping ability of ACE2 were integrated into a hybrid SERS substrate [131]. The resulting Fe_3O_4-Au-ACE2-virus nanocomposites enables the immediate detection of inactivated SARS-CoV-2 virus (Fig. 5(c)). Similarly, Fe_3O_4-WO_{3-X}@Au NPs integrated magnetic enrichment, fast clean-up separation, and synergistic enhancement of plasmons and CT for rapid quantification of analyte [132]. Conventional SERS substrates are passive nanoparticles that lack controllability and adaptability for precise and targeted sensing over small areas. Ma et al. reported a "rod-like" magnetic nanomotor-based SERS probe (MNM-SP), which consists of silica-coated Fe_3O_4 NPs [133]. Ag NPs were grown on the silica-coated surface to provide SERS "hot spots" for the nanomotors. The MNM-SP is driven by gradient and rotating magnetic fields. This enables it to precisely approach the target site and actively rotate to enhance contact with the analyte. Consequently, it provides directionally-enhanced SERS sensing through remote operation. Similarly, a nano-enzymatic magnetic nanomotor with a core-island structure consists of magnetic Fe_3O_4 cores and surface-modified Au islands [134]. This nano-enzymatic magnetic nanomotor can be controlled by an external magnetic field, enabling efficient collection of intracellular analytes for SERS sensing.

3 Advantages of SERS in diagnosis of cancer and pathogens

Currently, numerous biosensing platforms have been employed to detect cancer and infection-related targets, such as cancer biomarkers, cancer cells, and microorganisms. Radioisotope immunoassays (RIA) were once considered promising tools for disease diagnosis [135]. However, due to environmental health and safety risks, expensive specialized laboratory equipment, and waste disposal routes for radioactive materials, their application in clinical

practice has gradually declined. Enzyme-linked immunosorbent assay (ELISA) employs enzyme as the reporter to analyze biomarker [136, 137]. It is a safer, simpler, faster, and gold standard technique. However, the high cost of commercial ELISA test kit and the long analysis time have been barriers to the wider usage of ELISA. In addition, they are usually unable to distinguish the biomarker with low concentration and live/dead pathogens. Fluorescence immunoassay (FIA) is a highly sensitive approach commonly used to detect disease biomarkers at clinically desirable LOD due to the large absorption cross-section of fluorescence [138]. It is not surprising that FIA has several drawbacks. These include difficulty in identifying or labelling the target analyte, limited multiplexing due to frequent overlap of spectra caused by excessively broad emission bands, photobleaching, and non-specific binding, especially at low analyte levels. SERS is a surface sensitive technology that has been used for both quantitative and qualitative biosensing researches. SERS-based platforms have demonstrated a number of unique advantages in the field of cancer and pathogen diagnostics. As follows: (1) The detection of robust SERS signals from biomarkers at femtomolar concentrations represents a significant advance in biomedical detection technology, exceeding the detection limits of numerous existing techniques such as electrochemical, fluorescence, magnetic resonance imaging, positron emission tomography, and X-ray computed tomography. (2) SERS offers a unique fingerprint for each analyte, displaying narrow and sharp emission peaks that enable differentiation between samples. This distinctive property allows SERS technology to effectively identify biomarkers in complex biological mixtures. (3) By designing particles with different SERS signatures, it is possible to excite them simultaneously using a single laser beam. The signals emitted by these particles are spectrally proximate with subtle frequency variations. This attribute permits these nanoparticles to be multiplexed using rather simple instrumentation, allowing for the simultaneous detection of multiple distinct signals within a single detection system. (4) In contrast to infrared spectroscopy, Raman spectroscopy is particularly well-suited to medical diagnostic applications, as it exhibits minimal interference from water [139]. (5) Raman scattering differs from fluorescence in that it is an almost instantaneous process, which allows the excitation energy to be relaxed at significantly faster rates [140]. Consequently, the SERS signals are significantly more stable against photodegradation or photobleaching. Furthermore, the peak width of the Raman signal is approximately 10–100 times narrower than that of the fluorescence emission from organic dyes or quantum dots.

4 Applications of SERS in diagnosis of cancer and pathogens

Cancer and infectious diseases are two of the major public health problems and a major economic burden in the world [19]. World Health Organization (WHO) statistics show that both cancer and infectious diseases are closely linked to the leading causes of death worldwide [141]. Diagnosing disease early, quickly and accurately is key to guiding treatment and increasing patient survival. In recent years, the development of molecular biosensing platforms has focused on meeting the growing demands of cancer and pathogen diagnostics. Among these biosensing platforms, SERS offers several advantages, including ultra-sensitivity, high multiplexing capability, good photostability, and less interference from cell or tissue fluorescence [142–144]. There are two main detection methods that are typically adopted for SERS: label-free sensing and label-based SERS Sensing [145]. The label-free SERS detection strategy involves the direct adsorption of the target analyte onto the surface of the SERS substrate and the resulting spectral bands provide detailed intrinsic structural information and dynamics of the biomolecules attached to the substrate [146]. This strategy can provide detailed information on biomarkers, cells, and their interactions, which can guide the diagnosis of cancers and pathogens and reveal target composition and disease mechanisms [96, 122, 147]. SERS tags typically comprise of SERS-activated nanoparticles decorated with Raman reporter molecules that emit a strong and distinct Raman signal. By coupling recognition elements such as antibodies, enzymes, or aptamers to bind to epitopes of specific target analytes (e.g. metabolites, nucleic acids, or bacteria), SERS tags can be effectively applied as optical labelling tools for indirect sensing of target biomolecules *in vitro* and *in vivo* [148]. Taking advantage of its unique nature and integrated sensing capabilities, research reports on SERS applications in cancer and pathogenic diagnostics have increased exponentially in recent years. Notably, AI technology and microfluidic device-aided SERS technology have also shown great potential in cancer and pathogen diagnostic applications in recent years. This section will focus on the development of label-free sensing and Label-based sensing in cancer and pathogen diagnostics, as well as the new opportunities presented by AI and microfluidic device-aided SERS sensing.

4.1 Label-free SERS sensing

Between the two SERS methods, label-free SERS sensing has an advantage as it simplifies sample processing, reduces potential sources of interference, and avoids additional costs and complexity that labels may introduce [149]. At the same time, label-free SERS sensing also contributes to more accurate sample analysis and more reliable results by more directly reflecting the chemical composition and structural information of the target analyte itself.

SERS fingerprinting has great potential for identifying cancer and pathogen biomarkers from complex biological samples. For example, Ray et al. reported a hybrid SERS sensors consisting of graphene oxide attached to popcorn-shaped Au NPs, which is capable of ultra-sensitive label-free SERS detection of human immunodeficiency virus (HIV) DNA and bacteria and provides their chemical fingerprints [150]. The graphene oxide in this hybrid SERS substrate can enhance the Raman signal through CM, while the popcorn-shaped Au NPs can amplify the Raman signal through high EM enhancement due to their sharp tips. Additionally, the popcorn-shaped Au NPs can be effectively employed as a reaction site for selective binding to specific DNA or bacteria. Similarly, Petti et al. prepared a novel plasmonic nanostructure featuring a high-density array of inverted pyramid-shaped Au nanopores [149]. The abundant "hot spots" and small pyramidal area of this nanostructure facilitated virus detection. Further experimental results demonstrated that this SERS substrate can rapidly and highly sensitively detect hepatitis A virus (HAV) in water, with a LOD as low as 13 pg/mL (Fig. 6(a)). Lee et al. fabricated solid SERS probe for pancreatic cancer and prostate cancer diagnosis using 3D Ag nanowires (Ag NWs) densely stacked on glass fiber filters (GFF) [151]. The porous structure and large surface area of the Ag NWs-GFF contribute to the high uptake rate of urine. The nanogaps and nano-junctions of the crossed Ag NWs can function as "hot spots", and the 3D matrix of Ag NWs can significantly improve the SERS

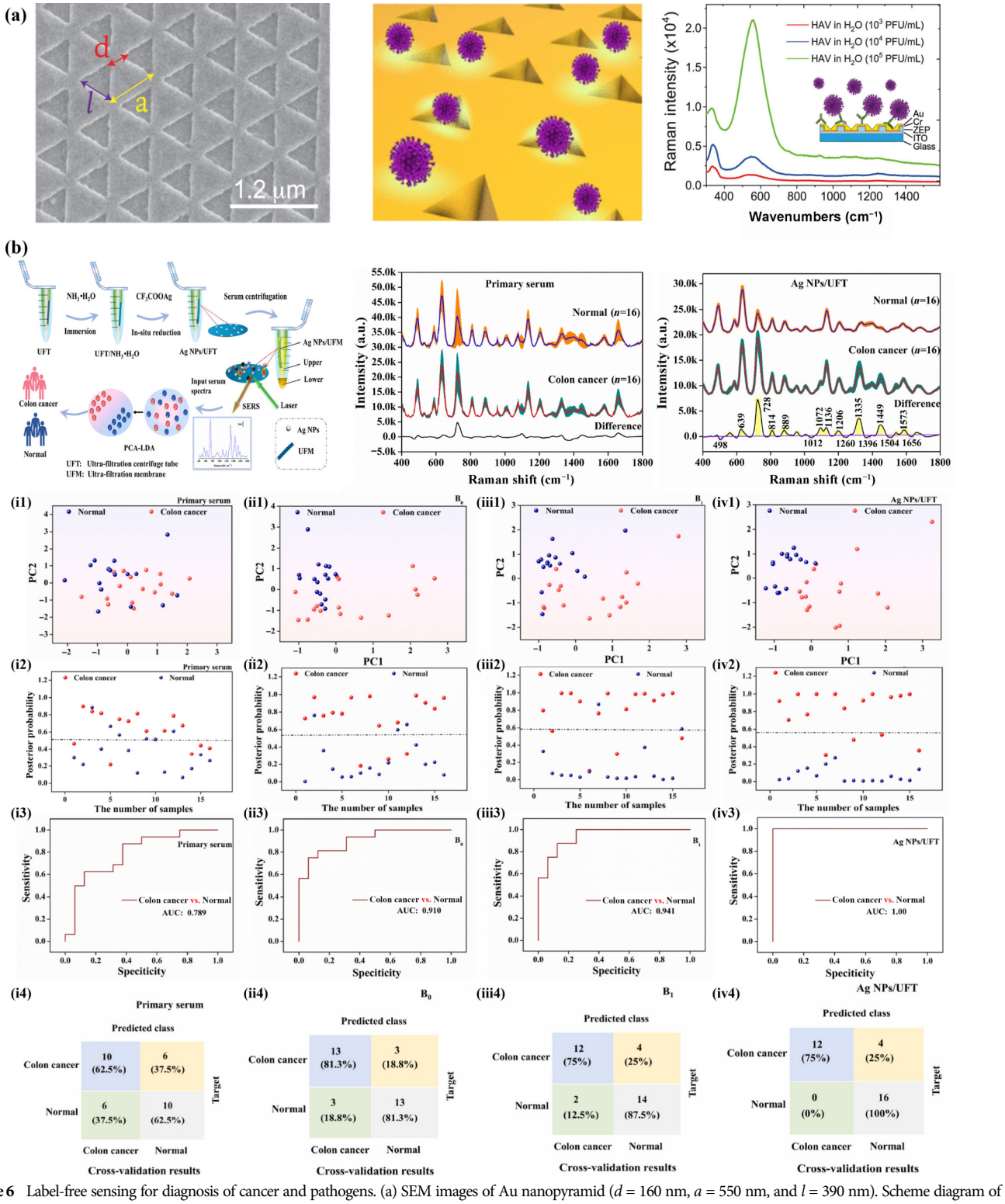

Figure 6 Label-free sensing for diagnosis of cancer and pathogens. (a) SEM images of Au nanopyramid (d = 160 nm, a = 550 nm, and l = 390 nm). Scheme diagram of the label-free pathogen detection based on Au nanopyramid. SERS spectra of the HAV virus in water (10^3–10^5 PFU/mL) adsorbed on the gold nanocavity pattern. Reproduced with permission from Ref. [149], © Palermo, G. et al. 2021. Published by American Chemical Society. (b) Scheme diagram for the preparation of Ag NPs/UFM and the combination of PCA-LDA algorithm for label-free detection of colon cancer. Average SERS spectra and difference spectra of colon cancer groups (n = 16) and normal groups (n = 16) Primary serum samples combined with Ag NPs colloids. Average SERS spectra and difference spectra of colon cancer groups (n = 16) and normal groups (n = 16) serum on its UFM after separation by filtration using Ag NPs/UFT biosensor. PCA-LDA analysis of four different ways of separating serum: (i1)–(iv1) Two-dimensional scatter plot of serum from the colon cancer and normal groups; (i2)–(iv2) posterior probability discriminant scatter plots of serum from the colon cancer and normal groups; (i3)–(iv3) ROC curves for cross-validation methods (AUC: area of integration under the ROC curve); (i4)–(iv4) confusion matrix of serum predicted outcomes in the colon cancer and normal groups. Reproduced with permission from Ref. [153], © Elsevier B.V. 2023.

effect by allowing additional "hot spots". This is reported to be the first label-free human urine SERS analysis for pancreatic cancer diagnosis. In addition, the researchers pointed out that early detection and monitoring of cancer could be greatly supported by combining the SERS sensor with a portable Raman device to monitor urine at home.

To improve the selectivity and specificity of cancer and pathogen detection, especially in complex biological samples, effective capture and immobilization of target analytes are critical. Park et al. fabricated high-density 3D arrays of Au NPs encapsulated in ultrathin hydrogel layer on filter paper [152]. During one-pot electrodeposition of Au grains onto hydrogel-encapsulated 3D Au electrodes, bacterial pathogen molecule (pyocyanin (PCN)) was trapped in the gaps between the Au nanostructures grown in the 3D hydrogel matrix, significantly enhancing the Raman signal intensity of PCN. In addition, the PCN remain trapped in the nanostructures during the washing process, allowing for the removal of interfering biomolecules from the culture medium without affecting the sensitivity of the SERS measurements. The integrity of the metal surface, even in the presence of complex culture media, is maintained by the hydrogel layer, which prevents the penetration of large adherent molecules. This SERS biosensor nanoplatform allows easy and direct monitoring of PCN concentrations during bacterial cultivation without the requirement for pre-processing steps. This is important for the early diagnosis of infections and the in-depth study of bacterial cell communication. In addition, the hierarchical nanostructure is designed by self-assembly between target-complementary DNA probe-conjugated Au NPs and head-flocked Au nanopillars in the presence of the targeted miRNAs [78]. This nanostructure generated a large number of 3D plasmonic "hot spots" that trigger extremely high amplification of SERS signals, achieving specific and ultra-sensitive detection of the target miRNAs (miR-10a and miR-21) in an LOD of 10 aM. Furthermore, clinical validation of the SERS sensor in urine samples demonstrated that it discriminated between prostate cancer (PC) patients and healthy controls with high diagnostic accuracy (0.93) due to the distinct expression levels of urinary exosomal miRNAs.

In practical applications for detecting and identifying cancer and pathogens, the concentration of target analytes is commonly low. Therefore, various strategies, such as filtration, magnetically assisted separation, and enrichment, are currently being developed to improve the accuracy and sensitivity of detection. Lu et al. employed a well-controlled "silver mirror reaction" to uniformly reduce Ag NPs on an ultrafiltration centrifuge tube (UFT) [153]. Subsequently, they exploited the ultrafiltration function of the Ag NPs/UFT SERS sensor to concentrate and isolate human serum, which not only overcomes the signal fluctuation problem of the label-free SERS assay based on the Ag NPs colloid, but also minimizes the interference of numerous small molecules and retains and concentrates proteins with high diagnostic value. The screening and diagnosis of colon cancer can be accurately performed by measuring the filtered serum with a portable Raman instrument and calculating it by means of a principal component analysis-linear discriminant analysis (PCA-LDA) model (Fig. 6(b)). This work introduces a novel combination of an ultrafiltration device, portable Raman, and multivariate data analysis, which is expected to offer potential in the field of non-invasive, rapid, and practical early cancer screening. Fang et al. proposed a method that integrates a low-cost thermophoretic enrichment strategy with SERS detection [154]. With the thermophoretic enrichment strategy, exosomes and Au NPs could be concentrated together in a small area of 500 μm within 10 min. *In situ* Raman signals of different exosomes derived from normal cells (293 cells), hepatoma cells (HuH-7 cells) and human serum exosomes are dynamically monitored with a detection limit of 1×10^2–1×10^3 particles/microliter, without the requirement for additional antibodies. By combining the SERS biosensor with MLAs, exosomes can be distinguished from normal cells and cancer cells with an accuracy of 100 percent. The researchers have concluded that this label-free SERS sensing technology provides a low-cost method for analyzing the Raman characteristics of exosomes, with potential for early cancer detection and *in-vitro* diagnosis.

4.2 Label-based SERS sensing

While label-free SERS sensing strategy is attractive for identifying analytes with large cross sections, the direct SERS detection of biomolecules with very small intrinsic Raman cross sections remains a real challenge in the biological analysis environment [33]. As a result, an indirect SERS detection strategy via SERS tags has been proposed and rapidly developed in recent years.

4.2.1 SERS tags

Typical SERS tags involve SERS-active nanomaterials, Raman reporter molecules, a protective layer, and target recognition molecules. The preceding section summarizes that nanomaterials with SERS activity have tunable SERS properties, which expands their potential applications. A crucial step in the preparation of SERS tags is the coupling of nanomaterials with SERS activity as SERS substrate with Raman reporter molecules, which generate strong characteristic Raman signals. Therefore, Raman reporter molecules should possess stable and strong Raman signals, clean spectral region with specific peaks, and the ability to bind to nanomaterials with SERS activity. Rh6G, CV, 4-aminothiophene (4-ATP), 5,5-dithiobis-2-nitrobenzoic acid (DTNB), and methylene blue (MB) are commonly selected as Raman reporter molecules for SERS labelling [155–159]. However, these molecules display multiple spectral bands in the fingerprint region, which can overlap with those of biomolecules and make them hard to discriminate. To solve this issue, several Raman reporter molecules that do not produce background interference have been reported, such as alkyne (C≡C) and nitrile (C≡N) [160–162]. These molecules exhibit single peaks in the Raman silent region (1800–2800 cm^{-1}), which reduces spectral confusion and background interference. This makes them a good choice for the analysis of biological samples. In addition, wrapping the nanostructure with a protective layer, such as silica, liposomes, polymers, or biomolecules, can improve the stability of SERS signals, enhance biocompatibility, and prevent nanoparticles from aggregating. Finally, recognition elements are introduced to identify target analytes. These can be categorized as: (1) Antibodies, which are Y-type proteins widely used for efficient and specific antigen recognition. However, they are commonly associated with low stability and high cost [163]. (2) Aptamers are DNA or RNA molecules that specifically bind to a target, providing inexpensive, stable and highly specific recognition. However, they are not as widely used as antibodies, particularly in clinical applications, because of limited target selection, cross-reactivity, and stability issues resulting from their small size [164]. (3) Antibiotics, used to inactivate or kill bacteria. Such capture elements also have the advantages of low cost, chemical stability, and high productivity,

but they are only specialized to identify different types of bacteria and have limited selectivity for different strains [165]. (4) Other recognition elements, such as transferrin, can also be applied for target capture due to the overexpression of the corresponding specific receptor on the surface of cancer cells [166, 167].

4.2.2 *SERS tags for diagnosis of cancer and pathogens*

In recent years, there has been considerable interest in applying SERS tags to the diagnosis of cancer and pathogens. Liu et al. developed an interference-free SERS platform with a sandwich structure [168]. This nanoplatform adopted a worm-like plasmonic Au film (pAu) as the SERS substrate and vancomycin-modified core-shell Prussian blue coated Au NPs (Au@PB@Van NPs) as the SERS tag. The pAu was modified with a hybrid self-assembled monolayer (SAM) containing 4-mercaptophenylboronic acid (4-MPBA) and 4-mercaptophenylbenzonitrile (4-MBN) (referred to as SAM/pAu). 4-MBN displays Raman peaks in the Raman silent region and acts as an internal reference probe. 4-MPBA serves as a trap to capture the bacteria on the pAu. Subsequently, the SERS tag Au@PB@Van NPs were bound to the captured bacteria, forming a sandwich structure of Au@PB@Van/bacteria/SAM/pAu. The detected SERS signal is derived from the Raman silent region and there is no background signal of biological origin, thus eliminating interference and improving the sensitivity and accuracy of the assay. This SERS biosensor allows for the capture and detection of *Staphylococcus aureus* (*S. aureus*) in whole blood samples. Additionally, the synergistic photothermal effect of pAu and Au@PB@Van NPs can achieve approximately 100% antimicrobial efficiency (Fig. 7(a)). Fan et al. developed a ratiometric SERS assay using two molecular beacons anchored on sea-urchinlike Au nanoclusters for quantitative detection of bladder cancer biomarker TK1 mRNA. This novel SERS biosensor was proven to be an effective tool in distinguishing bladder cancer cells from normal cells. Further clinical trials demonstrated the potential of the SERS biosensor for early non-invasive diagnosis of bladder tumor (BCa), with a sensitivity of 80% and a specificity of 100% [169]. The overexpression of β-galactosidase (SA-β-gal), which is a biomarker of cellular senescence and aberrant apoptosis, has been reported to be associated with cancer. You et al. prepared self-assembled Au nanostars on glass slides to form monolayers of Au NSs (Au-NF) [170]. The Au-NF were then modified with 4-mercaptophenylboronic acid (PMBA) to serve as a SERS substrate. The SERS labels were formed by PMBA and 4-aminothiophenol (PATP)-modified Au NSs. Lactose molecules acted as a bridge between the substrate and the SERS tag. This connection generated more "hot spots", greatly increasing the SERS signal intensity. The SERS biosensor enables highly sensitive and rapid detection of SA-β-gal and positively discriminates between cancer patient serum and normal human serum.

Magnetic nanoparticles (MNPs) are frequently employed to aid SERS tag for more efficient capture and subsequent accurate detection of target analytes in complex matrices. Zheng et al. designed a novel biosensor based on different morphologically controllable SERS tags using Raman reporter molecules and aptamers synergistically mediated by Au NRs [171]. The SERS tags exhibited cracked octahedral shapes and small protruding morphologies could achieve improved SERS sensitivity. Embedded Raman reporter molecules and anchored aptamers with specific biorecognition capabilities enable simultaneous detection of multiple pathogens without signal interference. The modified magnetic nanoparticles coupled with antibodies were used for specific separation and enrichment of the target pathogens *E. coli* O157:H7 and *S. typhimurium*. The SERS tags allowed simultaneous quantification of *E. coli* and *Salmonella typhimurium* in a range of 10 to 1×10^6 cfu/mL, with LOD of 5 and 8 cfu/mL, respectively. Kim et al. developed Au NPs-coated starch magnetic beads (Au NP@SMBs) to separate, concentrate and detect the target pathogen *E. coli* O157:H7, with LOD as low as a single cell [172]. The closely packed Au NPs on the surface of the beads provide an enhanced electromagnetic field, thereby amplifying the SERS signal in the presence of the target bacteria. The amplitude of the SERS signal is greatly enhanced by introducing SERS tags, which consist of Au NPs with specific antibodies immobilized by a bifunctional linking protein. This versatile SERS biosensor is expected to be a platform material for sensitive detection of target bacteria in various sample forms. This SERS biosensor could effectively separate and detect target bacteria, making it a promising platform material for the highly sensitive detection of target bacteria in a variety of sample forms. In addition, Zhou et al. designed a magnetically assisted sandwich-type SERS biosensor consisting of an SERS tag (robe DNA-conjugated DNA-engineered fractal gold nanoparticles, F-Au NPs) and a magnetic capture substrate (capture DNA-conjugated Ag-coated magnetic nanoparticles, Ag MNPs) [173]. This SERS biosensor enables multiplexed, ultrasensitive, highly selective and accurate detection of hepatocellular carcinoma (HCC)-associated three miRNAs (miRNA122, miRNA-223, and miRNA-21) in human serum, with great potential for the applications in cancer prediction, diagnosis, monitoring and staging.

Simultaneous detection of multiple target analytes can be achieved by designing SERS tags with multi-pathway detection capability using diverse Raman reporter molecules and diverse specific recognition elements. For instance, Gao et al. constructed an SERS chip with a sandwich structure [174]. This SERS chip comprises a plasmonic Au substrate coated with graphene and modified with phenylboronic acid (pAu/G/PBA), as well as two SERS tags consisting of a core (Au) and a shell (Prussian blue/poly-L-lysine and 4-mercaptobenzonitrile/polydopamine), both functionalized with aptamers (Au@PB@PLL@Apt and Au@MB@PDA@Apt). In this SERS platform, the detection signals depend on the distinctive and non-overlapping Raman bands of the SERS tags in the Raman silent region. This region does not produce any background signals from the sample matrix, resulting in enhanced detection sensitivity and accuracy. Moreover, the incorporation of high-affinity aptamers as recognition elements ensures the specific detection of the SERS chip. Based on this, a wide range of bacteria can be quickly and accurately identified and killed with the help of the SERS chip. Li et al. fabricated a novel hairpin self-assembly (CHA)-based SERS biosensor array for the simultaneous measurement of multiple cancer-related miRNAs in a sample [38]. The construction of the sensor array involved immobilizing one of four different hairpin-structured DNA sequences (hp1) onto one of four Au/Ag alloy NPs (AuAg NPs)-coated detection wells, each with a different sensing unit. The SERS tags, prepared by coupling AuAg NPs with a Raman reporter molecule of 4-mercaptobenzonitrile (MPBN) and the associated hairpin-structured DNA sequence 2 (hp2), were trapped on the corresponding sensor unit through a repeated specific CHA reaction when the target miRNA was present. The interactions between the SERS tags and the surface of the sensor coated with an AuAg NPs layer generated a large number of "hot spots", resulting

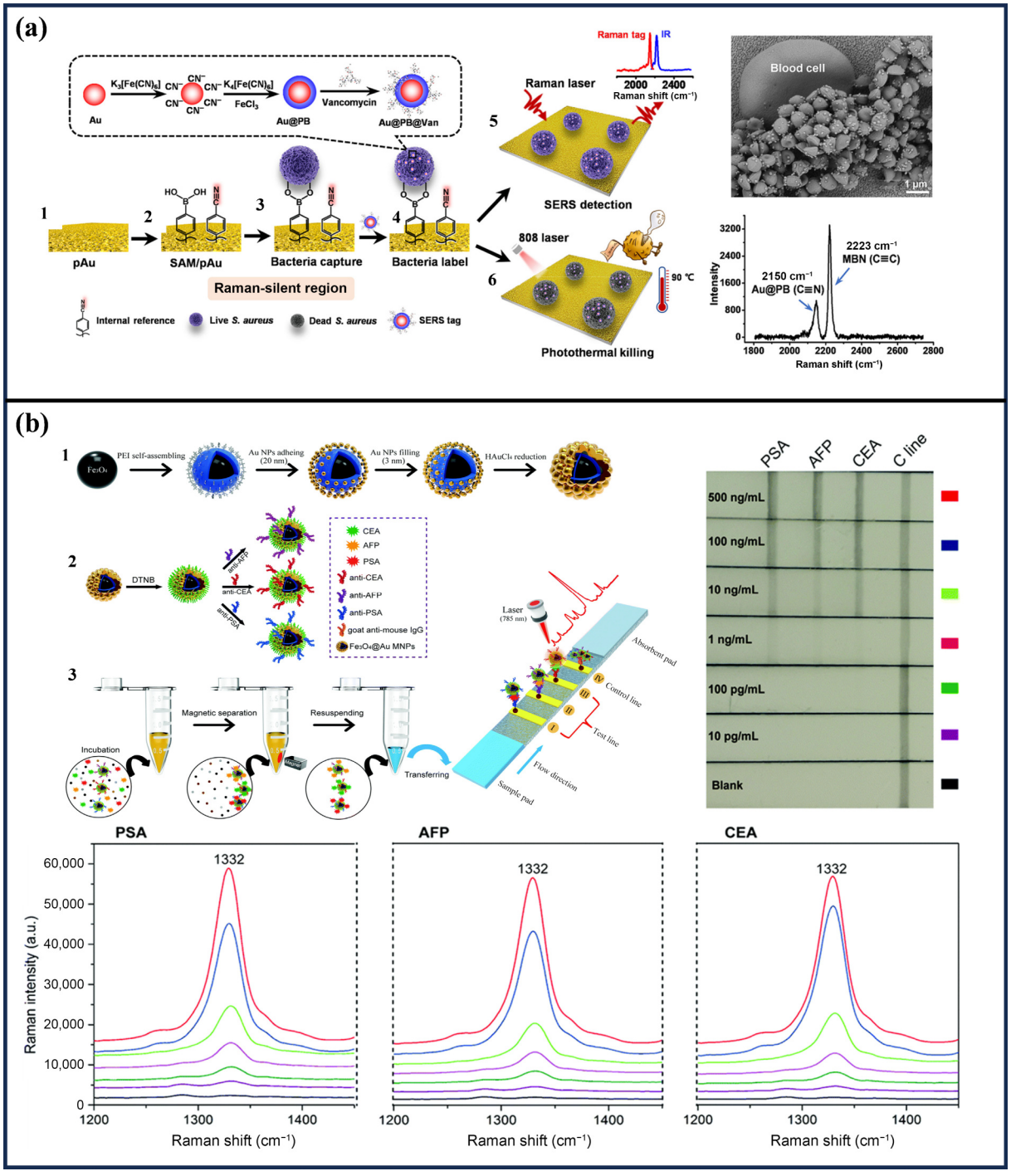

Figure 7 Label-based sensing for diagnosis of cancer and pathogens. (a) Illustration of the working principle of the present multifunctional SERS platform; SEM images, and the corresponding Raman spectra of the SERS substrate incubated with human blood containing *S. aureus* after a labeling process with Au@PB@Van NPs. Reproduced with permission from Ref. [168], © American Chemical Society 2020. (b) Schematic illustration of the synthetic process of RAuMNPs, antibody modified-RAuMNP SERS tag preparation, and RAuMNP tag-based LFIA for the simultaneous detection of three tumor biomarkers. Photographs of RAuMNP-based magnetic SERS-LFIA for PSA, AFP, and CEA detection in the serum sample. The average SERS spectrum of three T zones for different concentrations of PSA, AFP, and CEA. Reproduced with permission from Ref. [175], © The Royal Society of Chemistry 2020.

in a strong SERS signal that enabled the detection of the target miRNAs with a detection limit of 0.15 pM. Furthermore, the SERS sensor array successfully determined multiple cancer-associated miRNAs (miR-1246, miR-221, miR-133a, and miR-21) in buffer, serum, and cellular RNA extracts. Wang et al. proposed a new lateral flow immunoassay (LFIA) that employed raspberry-like Fe_3O_4@Au magnetic NPs (RAuMNPs) as a multifunctional SERS tag for the ultrasensitive and simultaneous quantification of multiple tumour biomarkers (Fig. 7(b)) [175]. RAuMNPs with raspberry-like morphology possess abundant hotspots and excellent magnetic properties. The NPs were functionalized with Raman reporter molecules and specific antibodies to enable magnetic

enrichment of target tumor biomarkers in serum and quantitative detection of targets on LFIA strips. By adopting this strategy, multiplexed analyses of three common tumor biomarkers on a single LFIA strip resulted in detection limits of 1.43 pg/mL for prostate specific antigen, 1.92 pg/mL for alpha-fetoprotein and 3.84 pg/mL for carcinoembryonic antigen. Label-based SERS sensing allows highly sensitive, multiplexed detection of target analytes. But it leads to the loss of the rich intrinsic biological information of the biological matrix. Additionally, the use of secondary labelled dyes significantly increases the total analysis time, reactant volume, and preparation steps. These limitations may restrict its application in high-throughput *in situ* cancer and pathogen diagnostics.

4.3 AI-aided SERS sensing

When diagnosing cancer or pathogens using label-free sensing, molecular vibrations may produce specific fingerprints that are difficult to recognize through manual visual inspection. Therefore, MLAs, as part of AI, has been integrated into SERS detection to identify features or perform classification. The efficiency of MLAs in extracting information from vibration spectra of complex mixtures or large datasets has enabled the translation of SERS from proof of concept to clinical application.

By combining SERS with MLAs, more efficient, accurate and deeper analysis of spectral data is possible. For instance, Zhao et al. exploited SiO_2-coated Ag NR arrays as an SERS substrate to discriminate and classify viral species, strains and variants by combining them with MLAs, including support vector machine (SVM), k-nearest neighbour, and random forests, and achieved > 99% discrimination accuracy [176]. SVM-based regression was used to construct quantitative calibration curves for accurately determining unknown virus concentrations in buffer and saliva. This SERS sensing platform enables precise classification and quantification of viruses in less than 20 min from sample preparation to diagnostic results. The integration of SERS and MLA method demonstrated the potential of their rapid virus detection and immediate diagnostic platforms by detecting and quantifying common respiratory viruses, including those that cause SARS-CoV-2. Pan et al. developed a label-free SERS substrate for clinical samples to capture bacteria and perform non-destructive detection in the saliva of patients with periodontal disease [177]. The SERS substrate was prepared with $NaBH_4$-reduced Ag NPs, and Na^+ was selected as an aggregating agent to provide "hot spots" for capturing bacteria, resulting in enhanced *porphyromonas gingivalis* (*P. gingivalis*) fingerprints. Combined with MLAs, four different oral bacteria including *P. gingivalis*, *Enterococcus faecalis* (*E. faecalis*), *S. aureus* and *Streptococcus mutans* (*S. mutans*) can be effectively classified. The researchers collected saliva from patients with clinical gingivitis and periodontitis and successfully identified the SERS signals of *P. gingivalis* in a complex oral environment (Fig. 8(a)). Jung et al. designed flexible and highly absorptive three-dimensional plasmonic hexaplex nanostructures (3D-PHP) coated on paper substrates [178]. These structures were integrated with a commercial saliva collection tube to create an efficient on-site sensing platform for lung cancer screening through SERS measurements of human saliva. The multispike hexaplex-shaped Au nanostructures improve contact with saliva viscosity, enabling efficient sampling and SERS enhancement. The 3D-PHP sensor was successfully used for lung cancer detection and diagnosis by testing patient saliva samples. A logistic regression-based ML model accurately classified patients as benign or malignant with high clinical sensitivity and specificity. Furthermore, the study investigated the locations of significant Raman peaks associated with different stages of lung cancer, providing new insights for early cancer diagnosis (Fig. 8(b)). Integrating the 3D-PHP sensor with a conventional saliva collection tube platform is expected to offer promising utility for rapid on-site disease screening and diagnosis, as well as significant advances in cancer detection and patient care.

4.4 Microfluidic-aided SERS sensing

The latest research in biosensing points to microfluidic chips as the most popular and widely used method for accurately preparing and treating detection samples. The integration of SERS with microfluidics has demonstrated several advantages. While the sensitivity of SERS in microfluidic devices is comparatively low in comparison to conventional macroscopic SERS platforms, the integration of SERS with microfluidics offers high-resolution, rapid, highly sensitive, non-destructive, *in-situ*, and multi-target microchip Raman detection with excellent reproducibility, providing new avenues for analytical platform integration, automation, and miniaturization [179, 180]. For instance, Qian et al. developed a pump-free, high-throughput microfluidic chip that employs catalytic hairpin assembly and hybridization chain reaction as a signal cascade amplification strategy for SERS detection [181]. This chip was comprised of six parallel functional units, which allowed the simultaneous analysis of multiple samples. The pump-free design and hydrophilic treatment had enabled the automated flow of reaction solutions in microchannels, removing the need for external heavy-duty pumps and significantly enhancing portability. This detection platform displayed low LOD for PIK3CA E542K (1.26 aM) and TP53 (2.04 aM) (two gastric cancer-related circulating tumor DNA (ctDNA)) of 1.26 aM and 2.04 aM, respectively. Moreover, the entire process was completed within an impressive 13 min. This system provided a valuable tool for analyzing ctDNA expression levels in real-time, which is beneficial for early cancer diagnosis. The SERS-coupled microfluidic platform designed by Kamińska et al. provided a powerful solution for identifying specific cancer cell lines [182]. It enabled monitoring of the expression levels of the cancer marker EpCAM in four target cancer cell lines: high (human metastatic prostate adenocarcinoma cells (LNCaP)), medium (human metastatic prostate adenocarcinoma cells (LNCaP)), weak (human metastatic prostate adenocarcinoma cells (LNCaP)), and no epithelial cell adhesion molecules (EpCAM) expressions (cervical cancer cells (HeLa)). This SERS-coupled microfluidic platform opened up a new avenue for early cancer diagnosis, identifying cell types by quantifying the levels of certain biomarkers on the cell surface. In addition to cellular research, SERS-coupled microfluidic platforms have been developed for the characterization and classification of pathogens. For instance, Sârbu et al. achieved fuzzy characterization and classification of bacterial species at the single-cell level using SERS technology, and the detection process was performed in a microfluidic device [183]. This Label-free SERS sensing enables the identification of bacterial species by comparing recorded raw spectra with detected spectra. However, the Raman spectra of pathogens are inherently weak and poorly defined, thus increasing the difficulty of label-free SERS detection. Chen et al. developed SERS probes tailored to selectively identify target microorganisms [184]. They then employed a microfluidic system to separate and isolate microbial samples and utilized SERS technology for high-

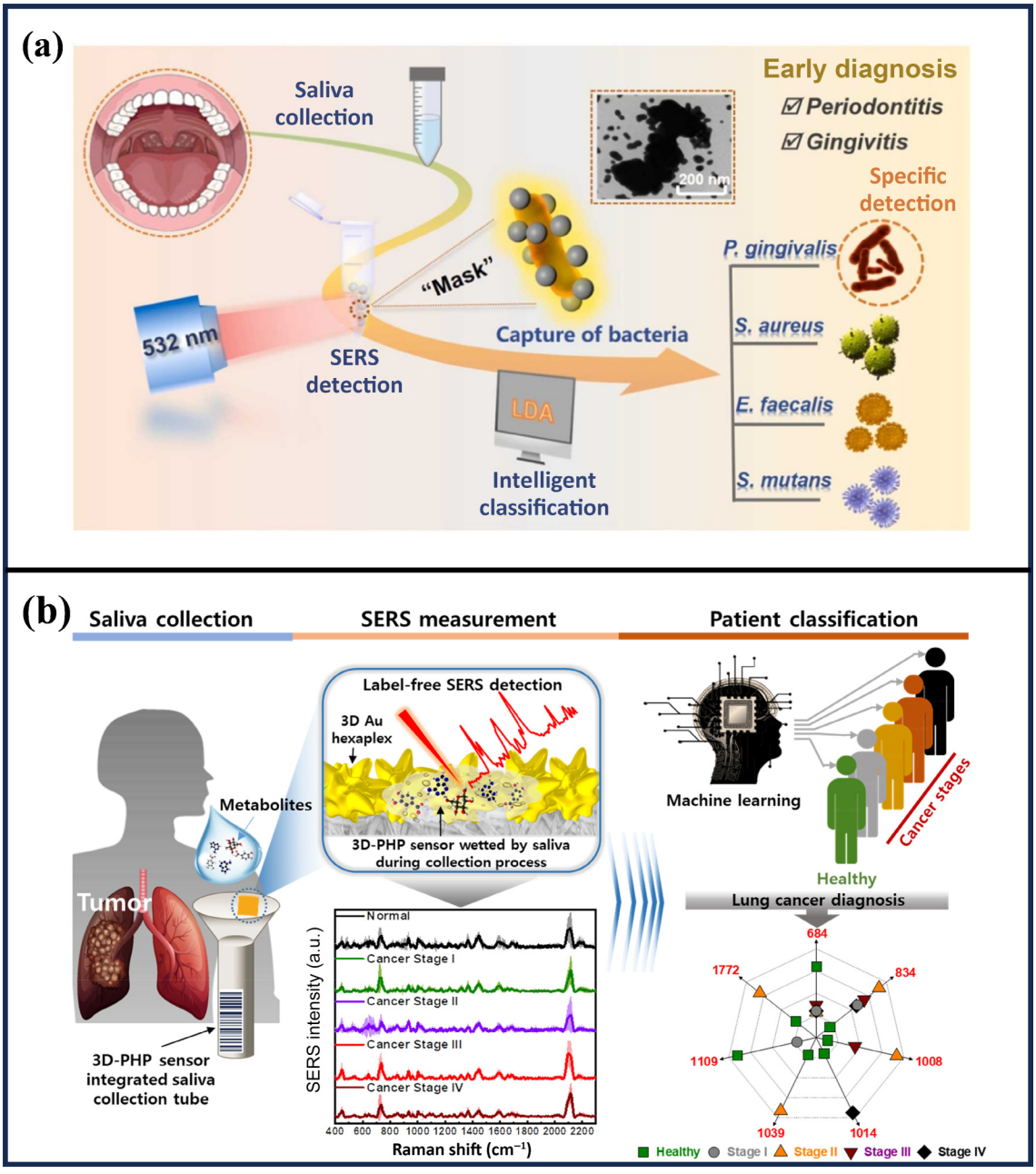

Figure 8 AI-aided SERS for diagnosis of cancer and pathogens. (a) Schematic illustration of the label-free SERS platform for clinical samples to capture bacteria and perform non-destructive detection in the saliva of patients with periodontal disease. Reproduced with permission from Ref. [177], © Elsevier B.V. 2024. (b) Schematic illustration of the 3D-PHP sensor integrated with saliva collection tube for applications in human saliva sensing and lung cancer diagnosis. Reproduced with permission from Ref. [178], © Linh, V. T. N. et al. 2023. Published by Elsevier B.V.

precision, quantitative analysis of microorganisms. It is worth noting that this SERS-microfluidic chip has been shown to accurately quantify yeast in a concentration range of 10^6 to 10^9 organisms/mL, with a maximum relative standard deviation of 5.6% from the concentration calibrated by the cultivation method. The results highlight the significant potential of this SERS-microfluidic chip for the rapid detection of a diverse range of microorganisms, including pathogenic bacteria and viruses.

5 Conclusions and prospects

Cancer and pathogens are currently the leading causes of death worldwide. Therefore, there is a critical need to develop simple, rapid, and effective diagnostic tools. Recent advances in optics and nanomaterials science have driven the development of surface-enhanced Raman spectroscopy (SERS), which shows great potential for disease diagnosis, including the detection of cancer cells, microbes and related biomarkers. In this review, we summarize recent advances in SERS technology for rapid, sensitive, and stable diagnosis of cancer and pathogens. In short, due to its high sensitivity, flexibility, SERS technology has become a promising platform for recognition and detection in both label-based and label-free applications in recent years. Considering the aforementioned progress in SERS-active nanomaterials, there are various directions for future development in this field with the goal of producing

more effective and desirable SERS substrates to meet increasingly demanding application requirements: (1) For the plasmonic metal SERS substrates, the key to their further development is to explore effective strategies to construct plasmonic nanostructures with highly ordered, uniform, and repeatable "hot spots" for reliable SERS detection. Thus, it would be of great interest to further develop simple, reliable and novel nanofabrication techniques to introduce smaller nano-gaps and generate more tightly packed "hot spots" on plasmonic metal SERS substrates. (2) For semiconductor nanomaterials, weak SERS activity has been a significant obstacle to their practical development. The development of integrated multiple nanomaterial engineering strategies is expected to optimize the SERS performance of semiconductor nanomaterials. The exploration of synergistic enhancement mechanisms and preparation methods for the integration of multiple materials engineering strategies is essential. (3) For metal/semiconductor nanocomposites, the combination of metal and semiconductor is one of the most effective ways to obtain ideal SERS substrates. The difficulty lies in how to effectively integrate the advantages of each component and fully exploit their multiple contributions to induce and enhance SERS signals through careful selection of functional components and rational design of composite structures. Metal/semiconductor SERS substrates can combine the inherent selectivity of strong EM enhancement and relatively weak CM enhancement, making the construction of such substrates an effective way to achieve highly sensitive and selective SERS enhancement. However, the currently developed approaches to composite SERS substrates all have their limitations and face many challenges, including controlled construction and complex mechanistic elucidation. (4) The design and development of SERS active nanomaterials also requires full consideration of their adaptability and applicability, which in most cases meet application-specific criteria. In direct SERS detection strategies, how to enhance the interaction between target molecules and SERS substrates is a major issue. In the label-based SERS detection strategy, the precise screening of affinity agents and Raman reporters in advance is the key to achieve accurate, effective and reliable SERS detection. These systems enable rapid detection of pathogens directly from complex samples without the need for purification or amplification steps. Antibodies have high binding affinity, but their large size makes them difficult to properly orient on SERS substrates and often interfere with the SERS spectra of target analytes. Aptamers and polymers offer greater versatility, smaller sizes, higher packing densities, minimal interference with SERS signatures and often lower production costs. (5) The development of portable and micro-SERS platforms is also important to extend the applicability of disease diagnosis to more realistic scenarios. While current efforts such as portable Raman device platforms allow for greater flexibility in disease diagnostics, traditional SERS technologies are widely used in cancer and pathogen diagnostics due to their superior SERS performance in terms of sensitivity, spectral resolution, and mapping capabilities. For example, portable devices have been successfully used to screen COVID-19 individuals in clinical breath samples or dengue virus in clinical blood samples [1]. This work has clearly demonstrated the effectiveness of portable devices in facilitating clinical translation and the great potential for the development of non-invasive human diagnostic tools for immediate detection or mass screening purposes. Therefore, further efforts are required to achieve the portability of disease diagnostics to meet clinical demands.

Data availability

Not applicable.

Acknowledgements

This work was supported by National Natural Science Foundation of China (Nos. 62401053 and 12374390), the Fundamental Research Funds for the Central Universities, the member of Youth Innovation Promotion Association Foundation of CAS, China (No. 2023310), and the Key Scientific and Technological Special Project of Ningbo City (No. 2023Z209).

Declaration of competing interest

The authors declare that they have no conflict of interest.

Author contribution statement

A. R. L. conceived the review topic. J. J. W. wrote the manuscript in consultation with all the other authors. B. H. Z., L. X., and Y. Y. Z. arranged all the figures. T. C., J. L., and A. R. L. modified the manuscript. All authors contributed to the final manuscript.

Informed consent

Not applicable.

Ethics statement

Not applicable.

Use of AI statement

None.

References

[1] Yuan, K. S.; Jurado-Sánchez, B.; Escarpa, A. Nanomaterials meet surface-enhanced Raman scattering towards enhanced clinical diagnosis: A review. *J. Nanobiotechnol.* **2022**, *20*, 537.

[2] Fitzgerald, R. C.; Antoniou, A. C.; Fruk, L.; Rosenfeld, N. The future of early cancer detection. *Nat. Med.* **2022**, *28*, 666–677.

[3] Lyu, N.; Pedersen, B.; Shklovskaya, E.; Rizos, H.; Molloy, M. P.; Wang, Y. L. SERS characterization of colorectal cancer cell surface markers upon anti-EGFR treatment. *Exploration* **2022**, *2*, 20210176.

[4] Zhang, Y. Q.; Liu, K. X.; Yu, J. K.; Chen, H. F.; Fu, R.; Zhu, S. Q.; Chen, Z. Q.; Wang, S. P.; Lu, S. Y. Single stain hyperspectral imaging for accurate fungal pathogens identification and quantification. *Nano Res.* **2022**, *15*, 6399–6406.

[5] Zhu, Y. Q.; Huang, W. Q.; Chen, G.; Xia, L.; You, Y. Z.; Yu, Y. Sticking-bacteria gel enhancing anti-multidrug-resistant microbial therapy under ultrasound. *Nano Res.* **2022**, *15*, 9105–9113.

[6] Ding, Y.; Chen, J. J.; Wu, Q.; Fang, B.; Ji, W. H.; Li, X.; Yu, C. M.; Wang, X. C.; Cheng, X. M.; Yu, H. D. et al. Artificial intelligence-assisted point-of-care testing system for ultrafast and quantitative detection of drug-resistant bacteria. *SmartMat* **2023**, *5*, e1214.

[7] Cialla-May, D.; Zheng, X. S.; Weber, K.; Popp, J. Recent progress in surface-enhanced Raman spectroscopy for biological and biomedical applications: From cells to clinics. *Chem. Soc. Rev.* **2017**, *46*, 3945–3961.

[8] Lu, L. Y.; Zhou, Y.; Zheng, T. T.; Tian, Y. SERS and EC dual-mode detection for dopamine based on WO_3–SnO_2 nanoflake arrays. *Nano Res.* **2023**, *16*, 4049–4054.

[9] Yang, Y. J.; Wu, S.; Chen, Y. L.; Ju, H. X. Surface-enhanced Raman scattering sensing for detection and mapping of key cellular biomarkers. *Chem. Sci.* **2023**, *14*, 12869–12882.

[10] Yang, B.; Wang, Y.; Guo, S.; Jin, S. L.; Park, E.; Chen, L.; Jung, Y. M. Charge transfer study for semiconductor and semiconductor/metal composites based on surface-enhanced Raman scattering. *Bull. Korean Chem. Soc.* **2021**, *42*, 1411–1418.

[11] Langer, J.; de Aberasturi, D. J.; Aizpurua, J.; Alvarez-Puebla, R. A.; Auguié, B.; Baumberg, J. J.; Bazan, G. C.; Bell, S. E. J.; Boisen, A.; Brolo, A. G. et al. Present and future of surface-enhanced Raman scattering. *ACS Nano* **2020**, *14*, 28–117.

[12] Smith, W. E. Practical understanding and use of surface enhanced Raman scattering/surface enhanced resonance Raman scattering in chemical and biological analysis. *Chem. Soc. Rev.* **2008**, *37*, 955–964.

[13] Haldavnekar, R.; Venkatakrishnan, K.; Tan, B. Non plasmonic semiconductor quantum SERS probe as a pathway for *in vitro* cancer detection. *Nat. Commun.* **2018**, *9*, 3065.

[14] Liu, Y.; Chui, K. K.; Xia, X.; Zhang, H.; Zhuo, X.; Wang, J. Selective deposition of a MOF at the spikes of Au nanostars for SERS detection. *Nano Res.* **2024**, *17*, 9166–9173.

[15] Qiu, C. G.; Zhang, W.; Zhou, Y. H.; Cui, H. W.; Xing, Y. L.; Yu, F. B.; Wang, R. Highly sensitive surface-enhanced Raman scattering (SERS) imaging for phenotypic diagnosis and therapeutic evaluation of breast cancer. *Chem. Eng. J.* **2023**, *459*, 141502.

[16] Awiaz, G.; Lin, J.; Wu, A. G. Recent advances of Au@Ag core-shell SERS-based biosensors. *Exploration* **2023**, *3*, 20220072.

[17] Tan, H. S.; Wang, T.; Sun, H. N.; Liu, A. H.; Li, S. S. Advances of surface-enhanced Raman spectroscopy in exosomal biomarkers analysis. *TrAC Trends Anal. Chem.* **2023**, *167*, 117253.

[18] Batool, S. M.; Yekula, A.; Khanna, P.; Hsia, T.; Gamblin, A. S.; Ekanayake, E.; Escobedo, A. K.; You, D. G.; Castro, C. M.; Im, H. et al. The liquid biopsy consortium: Challenges and opportunities for early cancer detection and monitoring. *Cell Rep. Med.* **2023**, *4*, 101198.

[19] Chisanga, M.; Muhamadali, H.; Ellis, D. L.; Goodacre, R. Enhancing disease diagnosis: Biomedical applications of surface-enhanced Raman scattering. *Appl. Sci.* **2019**, *9*, 1163.

[20] Ding, S. Y.; You, E. M.; Tian, Z. Q.; Moskovits, M. Electromagnetic theories of surface-enhanced Raman spectroscopy. *Chem. Soc. Rev.* **2017**, *46*, 4042–4076.

[21] Liu, B.; Thielert, B.; Reutter, A.; Stosch, R.; Lemmens, P. Quantifying the contribution of chemical enhancement to SERS: A model based on the analysis of light-induced degradation processes. *J. Phys. Chem. C* **2019**, *123*, 19119–19124.

[22] Jin, J.; Guo, Z. N.; Fan, D. Y.; Zhao, B. Spotting the driving forces for SERS of two-dimensional nanomaterials. *Mater. Horiz.* **2023**, *10*, 1087–1104.

[23] Lan, L. L.; Gao, Y. M.; Fan, X. C.; Li, M. Z.; Hao, Q.; Qiu, T. The origin of ultrasensitive SERS sensing beyond plasmonics. *Front. Phys.* **2021**, *16*, 43300.

[24] Fateixa, S.; Nogueira, H. I. S.; Trindade, T. Hybrid nanostructures for SERS: Materials development and chemical detection. *Phys. Chem. Chem. Phys.* **2015**, *17*, 21046–21071.

[25] Liu, Y. W.; Ma, H.; Han, X. X.; Zhao, B. Metal-semiconductor heterostructures for surface-enhanced Raman scattering: Synergistic contribution of plasmons and charge transfer. *Mater. Horiz.* **2021**, *8*, 370–382.

[26] Gahlaut, S. K.; Savargaonkar, D.; Sharan, C.; Yadav, S.; Mishra, P.; Singh, J. P. SERS platform for dengue diagnosis from clinical samples employing a hand held Raman spectrometer. *Anal. Chem.* **2020**, *92*, 2527–2534.

[27] Zhang, Y. Y.; Mi, X.; Tan, X. Y.; Xiang, R. Recent progress on liquid biopsy analysis using surface-enhanced Raman spectroscopy. *Theranostics* **2019**, *9*, 491–525.

[28] Blanco-Formoso, M.; Alvarez-Puebla, R. A. Cancer diagnosis through SERS and other related techniques. *Int. J. Mol. Sci.* **2020**, *21*, 2253.

[29] Wu, L.; Wang, Z. Y.; Zhang, Y. Z.; Fei, J. Y.; Chen, H.; Zong, S. F.; Cui, Y. P. *In situ* probing of cell-cell communications with surface-enhanced Raman scattering (SERS) nanoprobes and microfluidic networks for screening of immunotherapeutic drugs. *Nano Res.* **2017**, *10*, 584–594.

[30] Bodelón, G.; Montes-García, V.; López-Puente, V.; Hill, E. H.; Hamon, C.; Sanz-Ortiz, M. N.; Rodal-Cedeira, S.; Costas, C.; Celiksoy, S.; Pérez-Juste, I. et al. Detection and imaging of quorum sensing in *Pseudomonas aeruginosa* biofilm communities by surface-enhanced resonance Raman scattering. *Nat. Mater.* **2016**, *15*, 1203–1211.

[31] Sitjar, J.; Liao, J. D.; Lee, H.; Tsai, H. P.; Wang, J. R. Innovative and versatile surface-enhanced Raman spectroscopy-inspired approaches for viral detection leading to clinical applications: A review. *Anal. Chim. Acta* **2024**, *1325*, 342917.

[32] Constantinou, M.; Hadjigeorgiou, K.; Abalde-Cela, S.; Andreou, C. Label-free sensing with metal nanostructure-based surface-enhanced Raman spectroscopy for cancer diagnosis. *ACS Appl. Nano Mater.* **2022**, *5*, 12276–12299.

[33] Liu, H. Q.; Gao, X.; Xu, C.; Liu, D. B. SERS tags for biomedical detection and bioimaging. *Theranostics* **2022**, *12*, 1870–1903.

[34] Gong, T. X.; Das, C. M.; Yin, M. J.; Lv, T. R.; Singh, N. M.; Soehartono, A. M.; Singh, G.; An, Q. F.; Yong, K. T. Development of SERS tags for human diseases screening and detection. *Coord. Chem. Rev.* **2022**, *470*, 214711.

[35] de Aberasturi, D. J.; Henriksen-Lacey, M.; Litti, L.; Langer, J.; Liz-Marzán, L. M. Using SERS tags to image the three-dimensional structure of complex cell models. *Adv. Funct. Mater.* **2020**, *30*, 1909655.

[36] Huang, L. P.; Sun, H. W.; Sun, L. B.; Shi, K. Q.; Chen, Y. Z.; Ren, X. Q.; Ge, Y. C.; Jiang, D. F.; Liu, X. H.; Knoll, W. et al. Rapid, label-free histopathological diagnosis of liver cancer based on Raman spectroscopy and deep learning. *Nat. Commun.* **2023**, *14*, 48.

[37] Lee, S.; Jue, M.; Lee, K.; Paulson, B.; Oh, J.; Cho, M.; Kim, J. K. Early-stage diagnosis of bladder cancer using surface-enhanced Raman spectroscopy combined with machine learning algorithms in a rat model. *Biosens. Bioelectron.* **2024**, *246*, 115915.

[38] Si, Y. M.; Xu, L.; Deng, T.; Zheng, J.; Li, J. S. Catalytic hairpin self-assembly-based SERS sensor array for the simultaneous measurement of multiple cancer-associated miRNAs. *ACS Sens.* **2020**, *5*, 4009–4016.

[39] Wang, J.; Koo, K. M.; Trau, M. Tetraplex Immunophenotyping of cell surface proteomes via synthesized plasmonic nanotags and portable Raman spectroscopy. *Anal. Chem.* **2022**, *94*, 14906–14916.

[40] Gersten, J.; Nitzan, A. Electromagnetic theory of enhanced Raman scattering by molecules adsorbed on rough surfaces. *J. Chem. Phys.* **1980**, *73*, 3023–3037.

[41] Alonso-González, P.; Albella, P.; Schnell, M.; Chen, J.; Huth, F.; García-Etxarri, A.; Casanova, F.; Golmar, F.; Arzubiaga, L.; Hueso, L. E. et al. Resolving the electromagnetic mechanism of surface-enhanced light scattering at single hot spots. *Nat. Commun.* **2012**, *3*, 684.

[42] Li, A. R.; Isaacs, S.; Abdulhalim, I.; Li, S. Z. Ultrahigh enhancement of electromagnetic fields by exciting localized with extended surface plasmons. *J. Phys. Chem. C* **2015**, *119*, 19382–19389.

[43] Wang, X. T.; Ma, G. S.; Li, A. R.; Yu, J.; Yang, Z.; Lin, J.; Li, A.; Han, X. D.; Guo, L. Composition-adjustable Ag–Au substitutional alloy microcages enabling tunable Plasmon resonance for ultrasensitive SERS. *Chem. Sci.* **2018**, *9*, 4009–4015.

[44] Ding, S. Y.; Yi, J.; Li, J. F.; Ren, B.; Wu, D. Y.; Panneerselvam, R.;

Tian, Z. Q. Nanostructure-based plasmon-enhanced Raman spectroscopy for surface analysis of materials. *Nat. Rev. Mater.* **2016**, *1*, 16021.

[45] Johnson, P. B.; Christy, R. W. Optical constants of the noble metals. *Phys. Rev. B* **1972**, *6*, 4370–4379.

[46] Markin, A. V.; Markina, N. E.; Popp, J.; Cialla-May, D. Copper nanostructures for chemical analysis using surface-enhanced Raman spectroscopy. *TrAC Trends Anal. Chem.* **2018**, *108*, 247–259.

[47] Lay, C. L.; Koh, C. S. L.; Wang, J.; Lee, Y. H.; Jiang, R. B.; Yang, Y. J.; Yang, Z.; Phang, I. Y.; Ling, X. Y. Aluminum nanostructures with strong visible-range SERS activity for versatile micropatterning of molecular security labels. *Nanoscale* **2018**, *10*, 575–581.

[48] Tian, S.; Neumann, O.; McClain, M. J.; Yang, X.; Zhou, L. N.; Zhang, C.; Nordlander, P.; Halas, N. J. Aluminum nanocrystals: A sustainable substrate for quantitative SERS-based DNA detection. *Nano Lett.* **2017**, *17*, 5071–5077.

[49] Dörfer, T.; Schmitt, M.; Popp, J. Deep-UV surface-enhanced Raman scattering. *J. Raman Spectrosc.* **2007**, *38*, 1379–1382.

[50] Demirel, G.; Usta, H.; Yilmaz, M.; Celi, M.; Alidagi, H. A.; Buyukserin, F. Surface-enhanced Raman spectroscopy (SERS): An adventure from plasmonic metals to organic semiconductors as SERS platforms. *J. Mater. Chem. C* **2018**, *6*, 5314–5335.

[51] Zhao, Y.; Zhang, Y. J.; Meng, J. H.; Chen, S.; Panneerselvam, R.; Li, C. Y.; Jamali, S. B.; Li, X.; Yang, Z. L.; Li, J. F. et al. A facile method for the synthesis of large-size Ag nanoparticles as efficient SERS substrates. *J. Raman Spectrosc.* **2016**, *47*, 662–667.

[52] Sivapalan, S. T.; DeVetter, B. M.; Yang, T. K.; Van Dijk, T.; Schulmerich, M. V.; Carney, P. S.; Bhargava, R.; Murphy, C. J. Off-resonance surface-enhanced Raman spectroscopy from gold nanorod suspensions as a function of aspect ratio: Not what we thought. *ACS Nano* **2013**, *7*, 2099–2105.

[53] Liu, L.; Wu, Y. Z.; Yin, N. Q.; Zhang, H. M.; Ma, H. Silver nanocubes with high SERS performance. *J. Quant. Spectrosc. Radiat. Transfer* **2020**, *240*, 106682.

[54] Senthil Kumar, P.; Pastoriza-Santos, I.; Rodríguez-González, B.; Javier García de Abajo, F.; Liz-Marzán, L. M. High-yield synthesis and optical response of gold nanostars. *Nanotechnology* **2008**, *19*, 015606.

[55] Fan, M. K.; Lai, F. J.; Chou, H. L.; Lu, W. T.; Hwang, B. J.; Brolo, A. G. Surface-enhanced Raman scattering (SERS) from Au:Ag bimetallic nanoparticles: The effect of the molecular probe. *Chem. Sci.* **2013**, *4*, 509–515.

[56] Borah, R.; Verbruggen, S. W. Silver-gold bimetallic alloy versus core-shell nanoparticles: Implications for plasmonic enhancement and photothermal applications. *J. Phys. Chem. C* **2020**, *124*, 12081–12094.

[57] Li, S. Y.; Chen, J. J.; Xu, W. B.; Sun, B.; Wu, J. C.; Chen, Q.; Liang, P. Highly homogeneous bimetallic core-shell Au@Ag nanoparticles with embedded internal standard fabrication using a microreactor for reliable quantitative SERS detection. *Mater. Chem. Front.* **2023**, *7*, 1100–1109.

[58] Park, S.; Yang, P. X.; Corredor, P.; Weaver, M. J. Transition metal-coated nanoparticle films: Vibrational characterization with surface-enhanced Raman scattering. *J. Am. Chem. Soc.* **2002**, *124*, 2428–2429.

[59] Leung, L. W. H.; Weaver, M. J. Extending surface-enhanced Raman spectroscopy to transition-metal surfaces: Carbon monoxide adsorption and electrooxidation on platinum- and palladium-coated gold electrodes. *J. Am. Chem. Soc.* **1987**, *109*, 5113–5119.

[60] Tian, Z. Q.; Ren, B.; Li, J. F.; Yang, Z. L. Expanding generality of surface-enhanced Raman spectroscopy with borrowing SERS activity strategy. *Chem. Commun.* **2007**, 3514–3534.

[61] Lin, S. C.; Ze, H.; Zhang, X. G.; Zhang, Y. J.; Song, J.; Zhang, H. M.; Zhong, H. L.; Yang, Z. L.; Yang, C. Y.; Li, J. F. et al. Direct and simultaneous identification of multiple mitochondrial reactive oxygen species in living cells using a SERS borrowing strategy. *Angew. Chem., Int. Ed.* **2022**, *61*, e202203511.

[62] Ze, H.; Chen, X.; Wang, X. T.; Wang, Y. H.; Chen, Q. Q.; Lin, J. S.; Zhang, Y. J.; Zhang, X. G.; Tian, Z. Q.; Li, J. F. Molecular insight of the critical role of Ni in Pt-based nanocatalysts for improving the oxygen reduction reaction probed using an *in situ* SERS borrowing strategy. *J. Am. Chem. Soc.* **2021**, *143*, 1318–1322.

[63] Liu, Y.; Lyu, N.; Rajendran, V. K.; Piper, J.; Rodger, A.; Wang, Y. L. Sensitive and direct DNA mutation detection by surface-enhanced Raman spectroscopy using rational designed and tunable plasmonic nanostructures. *Anal. Chem.* **2020**, *92*, 5708–5716.

[64] Li, A. R.; Li, S. Z. Large-volume hot spots in gold spiky nanoparticle dimers for high-performance surface-enhanced spectroscopy. *Nanoscale* **2014**, *6*, 12921–12928.

[65] Srivastava, S. K.; Li, A. R.; Li, S. Z.; Abdulhalim, I. Optimal interparticle gap for ultrahigh field enhancement by LSP excitation via ESPs and confirmation using SERS. *J. Phys. Chem. C* **2016**, *120*, 28735–28742.

[66] Li, A. R.; Srivastava, S. K.; Abdulhalim, I.; Li, S. Z. Engineering the hot spots in squared arrays of gold nanoparticles on a silver film. *Nanoscale* **2016**, *8*, 15658–15664.

[67] Hao, E. C.; Schatz, G. C. Electromagnetic fields around silver nanoparticles and dimers. *J. Chem. Phys.* **2004**, *120*, 357–366.

[68] Zhang, Z. L.; Yang, P. F.; Xu, H. X.; Zheng, H. R. Surface enhanced fluorescence and Raman scattering by gold nanoparticle dimers and trimers. *J. Appl. Phys.* **2013**, *113*, 033102.

[69] Camden, J. P.; Dieringer, J. A.; Wang, Y. M.; Masiello, D. J.; Marks, L. D.; Schatz, G. C.; Van Duyne, R. P. Probing the structure of single-molecule surface-enhanced Raman scattering hot spots. *J. Am. Chem. Soc.* **2008**, *130*, 12616–12617.

[70] Wang, D.; Shi, F. X.; Jose, J.; Hu, Y. F.; Zhang, C. C.; Zhu, A. N.; Grzeschik, R.; Schlücker, S.; Xie, W. *In situ* monitoring of palladium-catalyzed chemical reactions by nanogap-enhanced Raman scattering using single Pd cube dimers. *J. Am. Chem. Soc.* **2022**, *144*, 5003–5009.

[71] Tapio, K.; Mostafa, A.; Kanehira, Y.; Suma, A.; Dutta, A.; Bald, I. A versatile DNA origami-based plasmonic nanoantenna for label-free single-molecule surface-enhanced Raman spectroscopy. *ACS Nano* **2021**, *15*, 7065–7077.

[72] Severoni, E.; Maniappan, S.; Liz-Marzán, L. M.; Kumar, J.; de Abajo, F. J. G.; Galantini, L. Plasmon-enhanced optical chirality through hotspot formation in surfactant-directed self-assembly of gold nanorods. *ACS Nano* **2020**, *14*, 16712–16722.

[73] Wu, Y. X.; Yu, Q.; Joung, Y.; Jeon, C. S.; Lee, S.; Pyun, S. H.; Joo, S. W.; Chen, L. X.; Choo, J. Highly uniform self-assembly of gold nanoparticles by butanol-induced dehydration and its SERS applications in SARS-CoV-2 detection. *Anal. Chem.* **2023**, *95*, 12710–12718.

[74] Zhang, M. L.; Pan, J. L.; Xu, X. Y.; Fu, G. G.; Zhang, L.; Sun, P.; Yan, X.; Liu, F. M.; Wang, C. G.; Liu, X. M. et al. Gold-trisoctahedra-coated capillary-based SERS platform for microsampling and sensitive detection of trace fentanyl. *Anal. Chem.* **2022**, *94*, 4850–4858.

[75] Lin, S.; Hasi, W.; Lin, X.; Han, S. O. G. W.; Xiang, T.; Liang, S.; Wang, L. Lab-on-capillary platform for on-site quantitative SERS analysis of surface contaminants based on Au@4-MBA@Ag core-shell nanorods. *ACS Sens.* **2020**, *5*, 1465–1473.

[76] Chen, L. L.; Hu, C. Y.; Dong, Y. Y.; Li, Y. P.; Shi, Q. Q.; Liu, G. Y.; Long, R.; Xiong, Y. J. Tunable layered gold nanochips for high sensitivity and uniformity in SERS detection. *J. Phys. Chem. C* **2023**, *127*, 8167–8174.

[77] Liu, J. Q.; Chen, C. N.; Lu, J. X.; Wang, Y. L.; Zhai, J. T.; Zhao, H. K.; Lu, N. Template-confined assembly of Ag nanocubes: An

approach to fabricate SERS substrate with good performance. *Talanta* **2024**, *269*, 125442.

[78] Kim, W. H.; Lee, J. U.; Jeon, M. J.; Park, K. H.; Sim, S. J. Three-dimensional hierarchical plasmonic nano-architecture based label-free surface-enhanced Raman spectroscopy detection of urinary exosomal miRNA for clinical diagnosis of prostate cancer. *Biosens. Bioelectron.* **2022**, *205*, 114116.

[79] Dinish, U. S.; Yaw, F. C.; Agarwal, A.; Olivo, M. Development of highly reproducible nanogap SERS substrates: Comparative performance analysis and its application for glucose sensing. *Biosens. Bioelectron.* **2011**, *26*, 1987–1992.

[80] Ingram, W. M.; Han, C. Q.; Zhang, Q. J.; Zhao, Y. P. Optimization of Ag-coated polystyrene nanosphere substrates for quantitative surface-enhanced Raman spectroscopy analysis. *J. Phys. Chem. C* **2015**, *119*, 27639–27648.

[81] Lin, W. C.; Liao, L. S.; Chen, Y. H.; Chang, H. C.; Tsai, D. P.; Chiang, H. P. Size dependence of nanoparticle-SERS enhancement from silver film over nanosphere (AgFON) substrate. *Plasmonics* **2011**, *6*, 201–206.

[82] Jibin, K.; Babu V, R.; Jayasree, R. S. Graphene-gold nanohybrid-based surface-enhanced Raman scattering platform on a portable easy-to-use centrifugal prototype for liquid biopsy detection of circulating breast cancer cells. *ACS Sustainable Chem. Eng.* **2021**, *9*, 15496–15505.

[83] Han, X. X.; Ji, W.; Zhao, B.; Ozaki, Y. Semiconductor-enhanced Raman scattering: Active nanomaterials and applications. *Nanoscale* **2017**, *9*, 4847–4861.

[84] Meng, X. Y.; Qiu, L.; Xi, G. C.; Wang, X. T.; Guo, L. Smart design of high-performance surface-enhanced Raman scattering substrates. *SmartMat* **2021**, *2*, 466–487.

[85] Deneme, I.; Liman, G.; Can, A.; Demirel, G.; Usta, H. Enabling three-dimensional porous architectures via carbonyl functionalization and molecular-specific organic-SERS platforms. *Nat. Commun.* **2021**, *12*, 6119.

[86] Chen, Z. Y.; Su, L. J.; Ma, X. H.; Duan, Z. H.; Xiong, Y. H. A mixed valence state Mo-based metal-organic framework from photoactivation as a surface-enhanced Raman scattering substrate. *New J. Chem.* **2021**, *45*, 5121–5126.

[87] Sun, H. Z.; Song, G.; Gong, W. B.; Lu, W. B.; Cong, S.; Zhao, Z. G. Stabilizing photo-induced vacancy defects in MOF matrix for high-performance SERS detection. *Nano Res.* **2022**, *15*, 5347–5354.

[88] Wang, Y. F.; Sun, Z. H.; Hu, H. L.; Jing, S. Y.; Zhao, B.; Xu, W. Q.; Zhao, C.; Lombardi, J. R. Raman scattering study of molecules adsorbed on ZnS nanocrystals. *J. Raman Spectrosc.* **2007**, *38*, 34–38.

[89] Maznichenko, D.; Venkatakrishnan, K.; Tan, B. Stimulating multiple SERS mechanisms by a nanofibrous three-dimensional network structure of titanium dioxide (TiO_2). *J. Phys. Chem. C* **2013**, *117*, 578–583.

[90] Cong, S.; Yuan, Y. Y.; Chen, Z. G.; Hou, J. Y.; Yang, M.; Su, Y. L.; Zhang, Y. Y.; Li, L.; Li, Q. W.; Geng, F. X. et al. Noble metal-comparable SERS enhancement from semiconducting metal oxides by making oxygen vacancies. *Nat. Commun.* **2015**, *6*, 7800.

[91] Lombardi, J. R.; Birke, R. L. Theory of surface-enhanced Raman scattering in semiconductors. *J. Phys. Chem. C* **2014**, *118*, 11120–11130.

[92] Lippitsch, M. E. Ground-state charge transfer as a mechanism for surface-enhanced Raman scattering. *Phys. Rev. B* **1984**, *29*, 3101–3110.

[93] Jensen, L.; Aikens, C. M.; Schatz, G. C. Electronic structure methods for studying surface-enhanced Raman scattering. *Chem. Soc. Rev.* **2008**, *37*, 1061–1073.

[94] Lombardi, J. R.; Birke, R. L.; Lu, T. H.; Xu, J. Charge-transfer theory of surface enhanced Raman spectroscopy: Herzberg-teller contributions. *J. Chem. Phys.* **1986**, *84*, 4174–4180.

[95] Li, A. R.; Lin, J.; Huang, Z. N.; Wang, X. T.; Guo, L. Surface-enhanced Raman spectroscopy on amorphous semiconducting rhodium sulfide microbowl substrates. *iScience* **2018**, *10*, 1–10.

[96] Lin, J.; Ren, W. Z.; Li, A. R.; Yao, C. Y.; Chen, T. X.; Ma, X. H.; Wang, X. T.; Wu, A. G. Crystal-amorphous core-shell structure synergistically enabling TiO_2 nanoparticles' remarkable SERS sensitivity for cancer cell imaging. *ACS Appl. Mater. Interfaces* **2020**, *12*, 4204–4211.

[97] Li, A. R.; Yu, J.; Lin, J.; Chen, M.; Wang, X. T.; Guo, L. Increased O 2p state density enabling significant photoinduced charge transfer for surface-enhanced Raman scattering of amorphous $Zn(OH)_2$. *J. Phys. Chem. Lett.* **2020**, *11*, 1859–1866.

[98] Wu, H.; Wang, H.; Li, G. H. Metal oxide semiconductor SERS-active substrates by defect engineering. *Analyst* **2017**, *142*, 326–335.

[99] Lan, L. L.; Fan, X. C.; Zhao, C. Y.; Gao, J.; Qu, Z. W.; Song, W. Z.; Yao, H. R.; Li, M. Z.; Qiu, T. Two-dimensional MBenes with ordered metal vacancies for surface-enhanced Raman scattering. *Nanoscale* **2023**, *15*, 2779–2787.

[100] Zheng, Z. H.; Cong, S.; Gong, W. B.; Xuan, J. N.; Li, G. H.; Lu, W. B.; Geng, F. X.; Zhao, Z. G. Semiconductor SERS enhancement enabled by oxygen incorporation. *Nat. Commun.* **2017**, *8*, 1993.

[101] Jiang, L. L.; Hu, Y. L.; Zhang, H. N.; Luo, X. L.; Yuan, R.; Yang, X. Charge-transfer resonance and surface defect-dominated WO_3 hollow microspheres as SERS substrates for the miRNA 155 assay. *Anal. Chem.* **2022**, *94*, 6967–6975.

[102] Hu, Y.; Li, X. B.; Wang, W. W.; Deng, F.; Han, L.; Gao, X. M.; Feng, Z. J.; Chen, Z.; Huang, J. T.; Zeng, F. Y. et al. Bi and S Co-doping g-C_3N_4 to enhance internal electric field for robust photocatalytic degradation and H_2 production. *Chin. J. Struct. Chem.* **2022**, *41*, 2206069–2206078.

[103] Wen, S. S.; Mu, M.; Xie, Q. H.; Zhao, B.; Song, W. Investigation of sulfur doping in Mn–Co oxide nanotubes on surface-enhanced Raman scattering properties. *Anal. Chem.* **2022**, *94*, 5987–5995.

[104] Yang, L. L.; Peng, Y. S.; Yang, Y.; Liu, J. J.; Huang, H. L.; Yu, B. H.; Zhao, J. M.; Lu, Y. L.; Huang, Z. R.; Li, Z. Y. et al. A novel ultra-sensitive semiconductor SERS substrate boosted by the coupled resonance effect. *Adv. Sci.* **2019**, *6*, 1900310.

[105] Wang, Y. N.; Zhang, M.; Ma, H.; Su, H. Y.; Li, A. S.; Ruan, W. D.; Zhao, B. Surface plasmon resonance from gallium-doped zinc oxide nanoparticles and their electromagnetic enhancement contribution to surface-enhanced Raman scattering. *ACS Appl. Mater. Interfaces* **2021**, *13*, 35038–35045.

[106] Cheng, H. F.; Wen, M. C.; Ma, X. C.; Kuwahara, Y.; Mori, K.; Dai, Y.; Huang, B. B.; Yamashita, H. Hydrogen doped metal oxide semiconductors with exceptional and tunable localized surface plasmon resonances. *J. Am. Chem. Soc.* **2016**, *138*, 9316–9324.

[107] Cao, Y.; Gou, H. Q.; Zhu, P. F.; Jin, Z. L. Ingenious design of CoAl-LDH p-n heterojunction based on CuI as holes receptor for photocatalytic hydrogen evolution. *Chin. J. Struct. Chem.* **2022**, *41*, 2206079–2206085.

[108] Fan, H. N.; Luo, W. B.; Dou, S. X.; Zheng, Z. J. Advanced two-dimensional materials toward polysulfides regulation of metal-sulfur batteries. *SmartMat* **2023**, *4*, e1186.

[109] Yu, D. X.; Xu, L.; Zhang, H. Z.; Li, J.; Wang, W. E.; Yang, L. B.; Jiang, X.; Zhao, B. A new semiconductor-based SERS substrate with enhanced charge collection and improved carrier separation: CuO/TiO_2 p-n heterojunction. *Chin. Chem. Lett.* **2023**, *34*, 107771.

[110] Zhang, H. Z.; Tang, Y. M.; Wang, W. E.; Yu, D. X.; Yang, L. B.; Jiang, X.; Song, W.; Zhao, B. A new semiconductor heterojunction SERS substrate for ultra-sensitive detection of antibiotic residues in egg. *Food Chem.* **2024**, *431*, 137163.

[111] Tan, Y.; Ma, L. N.; Gao, Z. B.; Chen, M.; Chen, F. Two-dimensional heterostructure as a platform for surface-enhanced Raman scattering. *Nano Lett.* **2017**, *17*, 2621–2626.

[112] Ghopry, S. A.; Alamri, M. A.; Goul, R.; Sakidja, R.; Wu, J. Z.

Extraordinary sensitivity of surface-enhanced Raman spectroscopy of molecules on MoS_2 (WS_2) nanodomes/graphene van der Waals heterostructure substrates. *Adv. Opt. Mater.* **2019**, *7*, 1801249.

[113] Yin, Y.; Miao, P.; Zhang, Y. M.; Han, J. C.; Zhang, X. H.; Gong, Y.; Gu, L.; Xu, C. Y.; Yao, T.; Xu, P. et al. Significantly increased Raman enhancement on MoX_2 (X = S, Se) monolayers upon phase transition. *Adv. Funct. Mater.* **2017**, *27*, 1606694.

[114] Guan, H. M.; Yi, W. C.; Li, T.; Li, Y. H.; Li, J. F.; Bai, H.; Xi, G. C. Low temperature synthesis of plasmonic molybdenum nitride nanosheets for surface enhanced Raman scattering. *Nat. Commun.* **2020**, *11*, 3889.

[115] Ge, Y. C.; Wang, F.; Yang, Y.; Xu, Y.; Ye, Y.; Cai, Y.; Zhang, Q. W.; Cai, S. Y.; Jiang, D. F.; Liu, X. H. et al. Atomically thin $TaSe_2$ film as a high-performance substrate for surface-enhanced Raman scattering. *Small* **2022**, *18*, 2107027.

[116] Song, G.; Sun, H. Z.; Chen, J.; Chen, Z. G.; Liu, B. Y.; Liu, Z. H.; Cong, S.; Zhao, Z. G. Quantum effects enter semiconductor-based SERS: Multiresonant $MoO_3{\cdot}xH_2O$ quantum dots enabling direct, sensitive SERS detection of small inorganic molecules. *Anal. Chem.* **2022**, *94*, 5048–5054.

[117] Wang, X. T.; Shi, W. X.; Jin, Z.; Huang, W. F.; Lin, J.; Ma, G. S.; Li, S. Z.; Guo, L. Remarkable SERS activity observed from amorphous ZnO nanocages. *Angew. Chem., Int. Ed.* **2017**, *56*, 9851–9855.

[118] Ling, X.; Xie, L. M.; Fang, Y.; Xu, H.; Zhang, H. L.; Kong, J.; Dresselhaus, M. S.; Zhang, J.; Liu, Z. F. Can graphene be used as a substrate for Raman enhancement. *Nano Lett.* **2010**, *10*, 553–561.

[119] Fu, J. H.; Zhong, Z.; Xie, D.; Guo, Y. J.; Kong, D. X.; Zhao, Z. X.; Zhao, Z. X.; Li, M. SERS-Active MIL-100(Fe) sensory array for ultrasensitive and multiplex detection of VOCs. *Angew. Chem., Int. Ed.* **2020**, *59*, 20489–20498.

[120] Xu, J. T.; Cheng, C.; Shang, S. W.; Gao, W.; Zeng, P.; Jiang, S. X. Flexible, reusable SERS substrate derived from ZIF-67 by adjusting LUMO and HOMO and its application in identification of bacteria. *ACS Appl. Mater. Interfaces* **2020**, *12*, 49452–49463.

[121] Lin, J.; Yu, J.; Akakuru, O. U.; Wang, X. T.; Yuan, B.; Chen, T. X.; Guo, L.; Wu, A. G. Low temperature-boosted high efficiency photo-induced charge transfer for remarkable SERS activity of ZnO nanosheets. *Chem. Sci.* **2020**, *11*, 9414–9420.

[122] Meng, X. Y.; Yu, J.; Wu, J. J.; Wang, Y. N.; Song, X. Y.; Xu, Z. Y.; Li, A. R.; Qiu, L.; Lin, J.; Wang, X. T. Significant surface-enhanced Raman scattering effect of Ag-loaded iron hydroxide enabled by coordination effect between Ag and hydroxyl group. *Inorg. Chem. Front.* **2023**, *10*, 3648–3655.

[123] Zhang, X. K.; Lei, Z. H.; Pan, Z. H.; Hu, J. Q.; Tao, L. L.; Zheng, Z. Q.; Feng, X.; Xue, J. C.; Tao, L.; Zhao, Y. A general approach to hybrid platform of Au nanoparticles on monolayer semiconductor for ultrasensitive Raman enhancement of 2D materials and molecule detection. *J. Alloys Compd.* **2023**, *938*, 168468.

[124] Zhang, X. Y.; Han, D. L.; Pang, Z. Y.; Sun, Y. S.; Wang, Y. X.; Zhang, Y. J.; Yang, J. H.; Chen, L. Charge transfer in an ordered Ag/Cu_2S/4-MBA system based on surface-enhanced Raman scattering. *J. Phys. Chem. C* **2018**, *122*, 5599–5605.

[125] Wang, C.; Guo, X. F.; Fu, Q. TiO_2 Thickness-dependent charge transfer in an ordered Ag/TiO_2/Ni nanopillar arrays based on surface-enhanced Raman scattering. *Materials* **2022**, *15*, 3716.

[126] Yang, F. Y.; Gong, Y. Y.; Zhou, M.; He, X. F.; Niu, L. Y.; Li, C.; Liu, X. J. Spontaneous synthesis of Ag nanoparticles decorated ZnAl layered double hydroxides for synergistically improved SERS activity. *Appl. Surf. Sci.* **2023**, *612*, 155701.

[127] Ben-Jaber, S.; Peveler, W. J.; Quesada-Cabrera, R.; Cortés, E.; Sotelo-Vazquez, C.; Abdul-Karim, N.; Maier, S. A.; Parkin, I. P. Photo-induced enhanced Raman spectroscopy for universal ultra-trace detection of explosives, pollutants and biomolecules. *Nat. Commun.* **2016**, *7*, 12189.

[128] Man, T. T.; Lai, W.; Xiao, M. S.; Wang, X. W.; Chandrasekaran, A. R.; Pei, H.; Li, L. A versatile biomolecular detection platform based on photo-induced enhanced Raman spectroscopy. *Biosens. Bioelectron.* **2020**, *147*, 111742.

[129] Guselnikova, O.; Lim, H.; Na, J.; Eguchi, M.; Kim, H. J.; Elashnikov, R.; Postnikov, P.; Svorcik, V.; Semyonov, O.; Miliutina, E. et al. Enantioselective SERS sensing of pseudoephedrine in blood plasma biomatrix by hierarchical mesoporous Au films coated with a homochiral MOF. *Biosens Bioelectron.* **2021**, *180*, 113109.

[130] Chen, X. Y.; Cui, A. R.; He, M. Y.; Yan, M.; Zhang, X. C.; Ruan, J.; Yang, S. K. Slippery Au nanosphere monolayers with analyte enrichment and SERS enhancement functions. *Nano Lett.* **2023**, *23*, 6736–6743.

[131] Li, Y. Y.; Lin, C. L.; Peng, Y. S.; He, J.; Yang, Y. High-sensitivity and point-of-care detection of SARS-CoV-2 from nasal and throat swabs by magnetic SERS biosensor. *Sens. Actuators B: Chem.* **2022**, *365*, 131974.

[132] Hu, W. Y.; Xia, L.; Hu, Y. F.; Li, G. K. Fe_3O_4–WO_{3-X}@AuNPs for magnetic separation, enrichment and surface-enhanced Raman scattering analysis all-in-one of albendazole and streptomycin in meat samples. *Sens. Actuators B: Chem.* **2024**, *402*, 135131.

[133] Wang, Y.; Liu, Y. H.; Li, Y.; Xu, D. D.; Pan, X.; Chen, Y. D.; Zhou, D. K.; Wang, B.; Feng, H. H.; Ma, X. Magnetic nanomotor-based maneuverable SERS probe. *Research* **2020**, *2020*, 7962024.

[134] Liu, S. M.; Xu, D. D.; Chen, J. L.; Peng, N.; Ma, T.; Liang, F. Nanozymatic magnetic nanomotors for enhancing photothermal therapy and targeting intracellular SERS sensing. *Nanoscale* **2023**, *15*, 12944–12953.

[135] Hanauske, A. R.; Arteaga, C. L.; Clark, G. M.; Buchok, J.; Marshall, M.; Hazarika, P.; Pardue, R. L.; Von Hoff, D. D. Determination of transforming growth factor activity in effusions from cancer patients. *Cancer* **1988**, *61*, 1832–1837.

[136] Lim, S.; Janzer, A.; Becker, A.; Zimmer, A.; Schüle, R.; Buettner, R.; Kirfel, J. Lysine-specific demethylase 1 (LSD1) is highly expressed in ER-negative breast cancers and a biomarker predicting aggressive biology. *Carcinogenesis* **2010**, *31*, 512–520.

[137] Kim, S. E.; Kim, Y. J.; Song, S. G.; Lee, K. N.; Seong, W. K. A simple electrochemical immunosensor platform for detection of Apolipoprotein A1 (Apo-A1) as a bladder cancer biomarker in urine. *Sens. Actuators B: Chem.* **2019**, *278*, 103–109.

[138] Zhu, Y. D.; Peng, J.; Jiang, L. P.; Zhu, J. J. Fluorescent immunosensor based on CuS nanoparticles for sensitive detection of cancer biomarker. *Analyst* **2014**, *139*, 649–655.

[139] Aroca, R. F.; Ross, D. J.; Domingo, C. Surface-enhanced infrared spectroscopy. *Appl. Spectrosc.* **2004**, *58*, 324A–338A.

[140] Doering, W. E.; Nie, S. M. Spectroscopic tags using dye embedded nanoparticles and surface-enhanced Raman scattering. *Anal. Chem.* **2003**, *75*, 6171–6176.

[141] Yuan, K. S.; Jiang, Z. J.; Jurado-Sánchez, B.; Escarpa, A. Nano/micromotors for diagnosis and therapy of cancer and infectious diseases. *Chem.-Eur. J.* **2020**, *26*, 2309–2326.

[142] Tahir, M. A.; Dina, N. E.; Cheng, H. Y.; Valev, V. K.; Zhang, L. W. Surface-enhanced Raman spectroscopy for bioanalysis and diagnosis. *Nanoscale* **2021**, *13*, 11593–11634.

[143] Lin, J.; Ma, X. H.; Li, A. R.; Akakuru, O. U.; Pan, C. S.; He, M.; Yao, C. Y.; Ren, W. Z.; Li, Y. Y.; Zhang, D. H. et al. Multiple valence states of Fe boosting SERS activity of Fe_3O_4 nanoparticles and enabling effective SERS-MRI bimodal cancer imaging. *Fundam. Res.* **2024**, *4*, 858–867.

[144] Lin, J.; Zhang, D. H.; Yu, J.; Pan, T.; Wu, X. X.; Chen, T. X.; Gao, C. Y.; Chen, C.; Wang, X. T.; Wu, A. G. Amorphous nitrogen-doped carbon nanocages with excellent SERS sensitivity and stability for accurate identification of tumor cells. *Anal. Chem.* **2023**, *95*, 4671–4681.

[145] Liu, Y.; Zhou, H. B.; Hu, Z. W.; Yu, G. X.; Yang, D. T.; Zhao, J. S. Label and label-free based surface-enhanced Raman scattering for pathogen bacteria detection: A review. *Biosens. Bioelectron.* **2017**, *94*, 131–140.

[146] Pérez-Jiménez, A. I.; Lyu, D. Y.; Lu, Z. X.; Liu, G. K.; Ren, B. Surface-enhanced Raman spectroscopy: Benefits, trade-offs and future developments. *Chem. Sci.* **2020**, *11*, 4563–4577.

[147] Chen, Y. P.; Chen, G.; Feng, S. Y.; Pan, J. J.; Zheng, X. W.; Su, Y.; Chen, Y.; Huang, Z. F.; Lin, X. Q.; Lan, F. H. et al. Label-free serum ribonucleic acid analysis for colorectal cancer detection by surface-enhanced Raman spectroscopy and multivariate analysis. *J. Biomed. Opt.* **2012**, *17*, 067003.

[148] Li, Y. E.; Wang, Z.; Mu, X. J.; Ma, A. N.; Guo, S. Raman tags: Novel optical probes for intracellular sensing and imaging. *Biotechnol. Adv.* **2017**, *35*, 168–177.

[149] Palermo, G.; Rippa, M.; Conti, Y.; Vestri, A.; Castagna, R.; Fusco, G.; Suffredini, E.; Zhou, J.; Zyss, J.; De Luca, A. et al. Plasmonic metasurfaces based on pyramidal nanoholes for high-efficiency SERS biosensing. *ACS Appl. Mater. Interfaces* **2021**, *13*, 43715–43725.

[150] Fan, Z.; Kanchanapally, R.; Ray, P. C. Hybrid graphene oxide based ultrasensitive SERS probe for label-free biosensing. *J. Phys. Chem. Lett.* **2013**, *4*, 3813–3818.

[151] Phyo, J. B.; Woo, A.; Yu, H. J.; Lim, K.; Cho, B. H.; Jung, H. S.; Lee, M. Y. Label-free SERS analysis of urine using a 3D-stacked AgNW-glass fiber filter sensor for the diagnosis of pancreatic cancer and prostate cancer. *Anal. Chem.* **2021**, *93*, 3778–3785.

[152] Kim, S.; Ansah, I. B.; Park, J. S.; Dang, H. J.; Choi, N.; Lee, W. C.; Lee, S. H.; Jung, H. S.; Kim, D. H.; Yoo, S. M. et al. Early and direct detection of bacterial signaling molecules through one-pot Au electrodeposition onto paper-based 3D SERS substrates. *Sens. Actuators B: Chem.* **2022**, *358*, 131504.

[153] You, R. Y.; Li, J.; Wang, H. N.; Wu, Y. L.; Weng, J. Z.; Lu, Y. D. High-performance SERS biosensor based on *in-situ* reduction of silver nanoparticles in an ultra-filtration centrifuge device for label-free detection of colon cancer in serum. *J. Membr. Sci.* **2023**, *678*, 121688.

[154] Guo, Y.; Zhang, R. Y.; You, H. J.; Fang, J. X. Effective enrichment of trace exosomes for the label-free SERS detection via low-cost thermophoretic profiling. *Biosens. Bioelectron.* **2024**, *253*, 116164.

[155] Jaworska, A.; Wojcik, T.; Malek, K.; Kwolek, U.; Kepczynski, M.; Ansary, A. A.; Chlopicki, S.; Baranska, M. Rhodamine 6G conjugated to gold nanoparticles as labels for both SERS and fluorescence studies on live endothelial cells. *Microchim. Acta* **2015**, *182*, 119–127.

[156] Yu, Q.; Wang, Y. Q.; Mei, R. C.; Yin, Y. C.; You, J. M.; Chen, L. X. Polystyrene encapsulated SERS tags as promising standard tools: Simple and universal in synthesis; highly sensitive and ultrastable for bioimaging. *Anal. Chem.* **2019**, *91*, 5270–5277.

[157] Yang, Y. T.; Hsu, I. L.; Cheng, T. Y.; Wu, W. J.; Lee, C. W.; Li, T. J.; Cheung, C. I.; Chin, Y. C.; Chen, H. C.; Chiu, Y. C. et al. Off-resonance SERS nanoprobe-targeted screen of biomarkers for antigens recognition of bladder normal and aggressive cancer cells. *Anal. Chem.* **2019**, *91*, 8213–8220.

[158] Song, D.; Yang, R.; Fang, S. Y.; Liu, Y. P.; Long, F.; Zhu, A. N. SERS based aptasensor for ochratoxin A by combining Fe_3O_4@Au magnetic nanoparticles and Au-DTNB@Ag nanoprobes with multiple signal enhancement. *Microchim. Acta* **2018**, *185*, 491.

[159] Simon, T.; Potara, M.; Gabudean, A. M.; Licarete, E.; Banciu, M.; Astilean, S. Designing theranostic agents based on pluronic stabilized gold nanoaggregates loaded with methylene blue for multimodal cell imaging and enhanced photodynamic therapy. *ACS Appl. Mater. Interfaces* **2015**, *7*, 16191–16201.

[160] Zhou, W.; Li, Q.; Liu, H. Q.; Yang, J.; Liu, D. B. Building Electromagnetic hot spots in living cells via target-triggered nanoparticle dimerization. *ACS Nano* **2017**, *11*, 3532–3541.

[161] Di, H. X.; Liu, H. Q.; Li, M. M.; Li, J.; Liu, D. B. High-precision profiling of sialic acid expression in cancer cells and tissues using background-free surface-enhanced Raman scattering tags. *Anal. Chem.* **2017**, *89*, 5874–5881.

[162] Yin, Y. M.; Li, Q.; Ma, S. S.; Liu, H. Q.; Dong, B.; Yang, J.; Liu, D. B. Prussian blue as a highly sensitive and background-free resonant Raman reporter. *Anal. Chem.* **2017**, *89*, 1551–1557.

[163] Pang, Y. F.; Wang, C. W.; Xiao, R.; Sun, Z. W. Dual-selective and dual-enhanced SERS nanoprobes strategy for circulating hepatocellular carcinoma cells detection. *Chem.-Eur. J.* **2018**, *24*, 7060–7067.

[164] Zou, Y. X.; Huang, S. Q.; Liao, Y. X.; Zhu, X. P.; Chen, Y. Q.; Chen, L.; Liu, F.; Hu, X. X.; Tu, H. J.; Zhang, L. et al. Isotopic graphene-isolated-Au-nanocrystals with cellular Raman-silent signals for cancer cell pattern recognition. *Chem. Sci.* **2018**, *9*, 2842–2849.

[165] Pang, Y. F.; Wan, N.; Shi, L. L.; Wang, C. W.; Sun, Z. W.; Xiao, R.; Wang, S. Q. Dual-recognition surface-enhanced Raman scattering (SERS) biosensor for pathogenic bacteria detection by using vancomycin-SERS tags and aptamer-Fe_3O_4@Au. *Anal. Chim. Acta* **2019**, *1077*, 288–296.

[166] Tang, R.; Hu, R.; Jiang, X. H.; Lu, F. LHRH-targeting surface-enhanced Raman scattering tags for the rapid detection of circulating tumor cells. *Sens. Actuators B: Chem.* **2019**, *284*, 468–474.

[167] Zhang, Q. N.; Li, J. S.; Tang, P.; Lu, X. X.; Tian, J. D.; Zhong, L. Y. Dynamic imaging of transferrin receptor molecules on single live cell with bridge gaps-enhanced Raman tags. *Nanomaterials* **2019**, *9*, 1373.

[168] Gao, X.; Yin, Y. L.; Wu, H. T.; Hao, Z.; Li, J. J.; Wang, S.; Liu, Y. Q. Integrated SERS platform for reliable detection and photothermal elimination of bacteria in whole blood samples. *Anal. Chem.* **2021**, *93*, 1569–1577.

[169] Liang, X.; Zhang, P.; Ma, M. H.; Yang, T.; Zhao, X. W.; Zhang, R.; Jing, M. X.; Song, R. D.; Wang, L.; Fan, J. H. Multiplex ratiometric gold nanoprobes based on surface-enhanced Raman scattering enable accurate molecular detection and imaging of bladder cancer. *Nano Res.* **2022**, *15*, 3487–3495.

[170] Han, S. R.; Fan, M.; Xu, G. C.; Liu, W. T.; Chen, J. B.; Lu, Y. D.; Feng, S. Y.; You, R. Y. Gold-nanostar-based surface-enhanced Raman scattering substrates for gastric carcinoma detection. *ACS Appl. Nano Mater.* **2022**, *5*, 12607–12615.

[171] Li, Y. Z.; Lu, C.; Zhou, S. S.; Fauconnier, M. L.; Gao, F.; Fan, B.; Lin, J. H.; Wang, F. Z.; Zheng, J. K. Sensitive and simultaneous detection of different pathogens by surface-enhanced Raman scattering based on aptamer and Raman reporter co-mediated gold tags. *Sens. Actuators B: Chem.* **2020**, *317*, 128182.

[172] You, S. M.; Luo, K.; Jung, J. Y.; Jeong, K. B.; Lee, E. S.; Oh, M. H.; Kim, Y. R. Gold nanoparticle-coated starch magnetic beads for the separation, concentration, and SERS-based detection of *E.* coli O157:H7. *ACS Appl. Mater. Interfaces* **2020**, *12*, 18292–18300.

[173] Wu, J. M.; Zhou, X.; Li, P.; Lin, X. L.; Wang, J. H.; Hu, Z. W.; Zhang, P. C.; Chen, D.; Cai, H. H.; Niessner, R. et al. Ultrasensitive and simultaneous SERS detection of multiplex MicroRNA using fractal gold nanotags for early diagnosis and prognosis of hepatocellular carcinoma. *Anal. Chem.* **2021**, *93*, 8799–8809.

[174] Zheng, S.; Xiao, J. R.; Zhang, J.; Sun, Q. X.; Liu, D. B.; Liu, Y. Q.; Gao, X. Python-assisted detection and photothermal inactivation of Salmonella typhimurium and Staphylococcus aureus on a background-free SERS chip. *Biosens. Bioelectron.* **2024**, *247*, 115913.

[175] Shen, W. Z.; Wang, C. W.; Yang, X. S.; Wang, C. G.; Zhou, Z. H.;

Liu, X. X.; Xiao, R.; Gu, B.; Wang, S. Q. Synthesis of raspberry-like nanogapped Fe_3O_4@Au nanocomposites for SERS-based lateral flow detection of multiple tumor biomarkers. *J. Mater. Chem. C* **2020**, *8*, 12854–12864.

[176] Yang, Y. J.; Xu, B. B.; Murray, J.; Haverstick, J.; Chen, X. Y.; Tripp, R. A.; Zhao, Y. P. Rapid and quantitative detection of respiratory viruses using surface-enhanced Raman spectroscopy and machine learning. *Biosens. Bioelectron.* **2022**, *217*, 114721.

[177] Zhang, T.; Xu, Z. M.; Liu, X.; Liu, L.; Jiang, S.; Zhang, Z.; Li, Y.; Pan, S. Activated silver nanoparticle-based platform for specific capture of *Porphyromonas gingivalis* in human saliva. *Sens. Actuators B: Chem.* **2024**, *403*, 135171.

[178] Linh, V. T. N.; Kim, H.; Lee, M. Y.; Mun, J.; Kim, Y.; Jeong, B. H.; Park, S. G.; Kim, D. H.; Rho, J.; Jung, H. S. 3D plasmonic hexaplex paper sensor for label-free human saliva sensing and machine learning-assisted early-stage lung cancer screening. *Biosens. Bioelectron.* **2024**, *244*, 115779.

[179] Pu, H. B.; Xiao, W.; Sun, D. W. SERS-microfluidic systems: A potential platform for rapid analysis of food contaminants. *Trends Food Sci. Technol.* **2017**, *70*, 114–126.

[180] Xie, Y. J.; Xu, L.; Zhang, J. H.; Zhang, C. G.; Hu, Y.; Zhang, Z. X.; Chen, G. X.; Qi, S. Y.; Xu, X. W.; Wang, J. et al. Precise diagnosis of tumor cells and hemocytes using ultrasensitive, stable, selective cuprous oxide composite SERS bioprobes assisted with high-efficiency separation microfluidic chips. *Mater. Horiz.* in press, DOI: 10.1039/D4MH00791C.

[181] Cao, X. W.; Ge, S. J.; Hua, W. W.; Zhou, X. Y.; Lu, W. B.; Gu, Y. Y.; Li, Z. Y.; Qian, Y. Y. A pump-free and high throughput microfluidic chip for highly sensitive SERS assay of gastric cancer related circulating tumor DNA via a cascade signal amplification strategy. *J. Nanobiotechnol.* **2022**, *20*, 271.

[182] Czaplicka, M.; Niciński, K.; Nowicka, A.; Szymborski, T.; Chmielewska, I.; Trzcińska-Danielewicz, J.; Girstun, A.; Kamińska, A. Effect of varying expression of EpCAM on the efficiency of CTCs detection by SERS-based immunomagnetic optofluidic device. *Cancers* **2020**, *12*, 3315.

[183] Dina, N. E.; Gherman, A. M. R.; Colniță, A.; Marconi, D.; Sârbu, C. Fuzzy characterization and classification of bacteria species detected at single-cell level by surface-enhanced Raman scattering. *Spectrochim. Acta A: Mol. Biomol. Spectrosc.* **2021**, *247*, 119149.

[184] Wen, P.; Yang, F.; Zhao, H. X.; Xu, Y.; Li, S. B.; Chen, L. Novel digital SERS-microfluidic chip for rapid and accurate quantification of microorganisms. *Anal. Chem.* **2024**, *96*, 1454–1461.